

UNCLASSIFIED

AD NUMBER

AD827214

LIMITATION CHANGES

TO:

Approved for public release; distribution is unlimited.

FROM:

Distribution authorized to U.S. Gov't. agencies and their contractors;
Administrative/Operational Use; SEP 1967. Other requests shall be referred to Army Research Office, Durham, NC.

AUTHORITY

ARO ltr 12 Aug 1971

THIS PAGE IS UNCLASSIFIED

4872.3-E

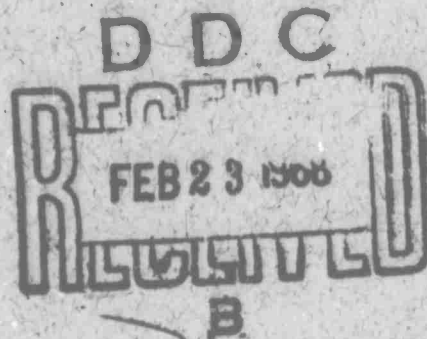
TP-67-16-T

AD827214

Low Cycle Fatigue Behavior Under Biaxial Strain Distribution

SEPTEMBER, 1967

PREPARED FOR
U.S. ARMY RESEARCH OFFICE — DURHAM
CONTRACT NO. DA-31-124 ARO-D-274



This document is subject to special export controls and each transmission to foreign governments or foreign nationals may be made only with prior approval of the U. S. Army Research Office—Durham, Durham, North Carolina.

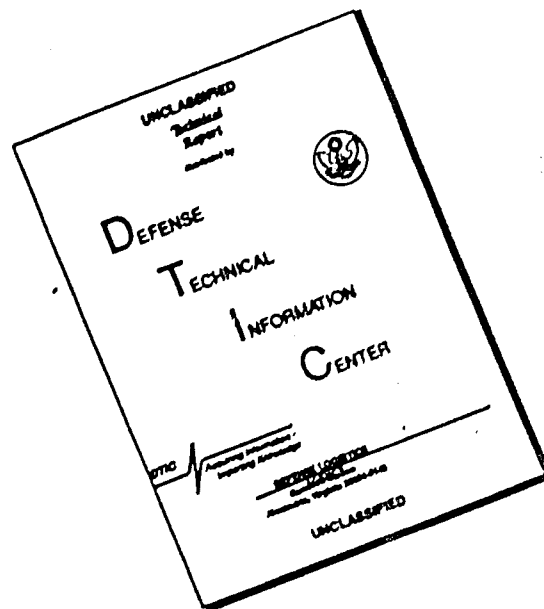
The findings in this report are not to be construed as an official Department of the Army position, unless so designated by other authorized documents.

Hamilton
Standard

U
A.
DIVISION OF UNITED AIRCRAFT CORPORATION

63

DISCLAIMER NOTICE



THIS DOCUMENT IS BEST QUALITY AVAILABLE. THE COPY FURNISHED TO DTIC CONTAINED A SIGNIFICANT NUMBER OF PAGES WHICH DO NOT REPRODUCE LEGIBLY.

**Hamilton
Standard**

U
DIVISION OF UNITED AIRCRAFT CORPORATION
A_®

TP-67-16-T

Hamilton Standard Division of United Aircraft Corporation

D. A. Project No. 20010501B700

"LOW CYCLE FATIGUE BEHAVIOR UNDER BIAXIAL STRAIN DISTRIBUTION"

Contract No. DA-31-124-ARO-D-274

September, 1967

Joseph L. Mattavi

Requests for additional copies by Agencies of the Department of Defense, their contractors, and other Government Agencies should be directed to:

Defense Documentation Center
Cameron Station
Alexandria, Virginia 22314

Department of Defense contractors must be established for DDC services or have their "need-to-know" certified by the cognizant military agency of their project or contract.

NOMENCLATURE

ϵ	conventional strain
$\bar{\epsilon}$	equivalent strain
σ	conventional stress
$\bar{\sigma}$	equivalent stress
a, ν	exponent expressing plastic strain-life dependency
b	exponent expressing elastic strain-life dependency
n	number of cycles accumulated at a given cyclic strain
	range
N	number of cycles to fracture at a given cyclic strain
	range
η	station designation in finite difference solution
C_e, C_p	constants
h	thickness of station
μ	poisson's ratio
E	modulus of elasticity
ρ	mass density
ω	angular velocity
i, j	positive integers

Subscripts

E	elastic
e	elastic range

NOMENCLATURE (Cont.)

f	fracture
m	mean
p	plastic
r	radial
T	total
Z	transverse
ult	ultimate
θ	circumferential

ABSTRACT

This paper presents a linear cumulative damage theory, macroscopically considering elastic and plastic straining, and accounting for biaxiality through the von Mises theory for combined strains. Experimentation on SAE 4340 steel alloy supported this damage hypothesis and confirmed the associated exponential relationship between elastic strains with cyclic life and plastic strains with cyclic life. A limited evaluation of an aluminum casting material, C-355-T61, also supported this exponential dependency. Notching did not significantly alter this low cycle fatigue behavior.

INTRODUCTION

Fracture investigation of structural members exposed to moderate-to-heavy loading results in the prominence of one fracture mechanism - fatigue. In view of the multi-variable dependency of this mechanism, preventive design has largely relied upon laboratory testing, supplemented by sound statistical interpretation of the results. This technique is still most often employed today in the high anticipated number of stress cycles spectra of the classic stress-number of cycles fatigue curve. There has evolved, however, a technique for analytically predicting material fatigue behavior in the low-cycle, high-load portion of the fatigue curve. Manson [1, 2] was responsible for establishing the relationship between cycle strain and cycles-to-fracture. This is stated mathematically in the following form.

$$\epsilon_p N^\nu = \text{Constant}, \quad (1)$$

where ϵ_p represents plastic strain range, N indicates cycles to fracture, and ν signifies exponential dependency. Coffin [3] experimentally determined this exponent to have a value of $1/2$ and applied the boundary condition that $\epsilon_p = 2\epsilon_f$ at $N = 1/4$ where ϵ_f represents strain at fracture or material ductility to obtain $C = \epsilon_f$. Although Coffin's initial work was conducted with copper, Coffin and Tavernelli [4, 5] demonstrated this exponential behavior, applied to an assortment of other metals including steel and aluminum alloys. This work supported the exponent value of $1/2$ in the majority of cases. Gross [6] stated that cyclic total strain, rather

INTRODUCTION (Cont.)

than cyclic plastic strain, is the significant value that yields the same relationship for many different materials when describing low cycle fatigue behavior. Gross's polymaterial power exponent was approximately $1/3$.

The test limitations of the cited works are twofold. First, the work was restricted to uniaxial loading, and second, the loading mode was completely reversed. Ives, Kooistra, and Tucker [7] have conducted low cycle biaxial fatigue tests on several pressure vessel steels but have not included effects of mean strain. There have been several papers [8, 9, 10, 11] written on uniaxial low cycle fatigue considering the effects of mean strain. These included several aluminum alloys and a pressure vessel steel. A requisite to properly evaluating the effect of mean strain is the establishment of a cumulative damage theory. Ohji, Miller, and Marin [11] explicitly proposed and experimentally supported a linear damage theory based on strain that is equivalent to Miner's classical theory [12]. Additional uniaxial cumulative damage investigations conducted in the low cycle fatigue regime are contained in references [13, 14, 15, 16]. Miner's theory applied to these studies resulted in fairly satisfactory results. All of the experimental activity conducted with regard to evaluating cumulative damage, however, was of a completely reversed straining nature, and, thus, excluded the contribution of mean strain.

INTRODUCTION (Cont.)

This present study's purpose was to evaluate low cycle fatigue behavior under a biaxial strain distribution with particular emphasis on mean strain and cumulative damage considerations. Additionally, it was considered highly desirable to select a loading mode that simulated loading of structural members more closely than previous specimen testing. The completely reversed strain cycling cited earlier requires reversal of the load vector. Loading of this nature is generally associated with vibratory modes, which implies high frequency of application or high cycle fatigue. The loading mode utilized in this study is representative of pressure loading and centrifugal loading and is particularly applicable to pressure vessels and rotating members.

THEORETICAL CONSIDERATIONS

Equation (1) can be rewritten as:

$$\epsilon_p^a N = C_p; a = 1/\nu \quad (2)$$

Although the majority of work has been conducted with emphasis on the plastic strain to life relationship, Manson [17] has shown that this same exponential relationship governs the elastic strain to life dependency, i.e.,

$$\epsilon_e^b N = C_e \quad (3)$$

where ϵ_e denotes elastic strain range and b the elastic exponent. Smith, Hirshberg, and Manson [18] proposed the following boundary condition based on 11 different alloys, including steel, aluminum, titanium, and

THEORETICAL CONSIDERATIONS (Cont.)

nickel, to obtain the constant C_e .

$$\epsilon_e = 0.9 \sigma_{ult} / E \quad \text{when } N = 10^5 \quad (4)$$

which results in
$$C_e = (0.9 \sigma_{ult} / E)^b 10^5 \quad (5)$$

A linear damage theory is proposed to include the elastic case by considering total damage per cycle as being composed of damage attributed to cyclic plastic strain and damage attributed to cyclic elastic strain. Damage per cycle is represented as ϵ_p^a and ϵ_e^b for the plastic and elastic cases, respectively. Total damage is expressed mathematically as

$$D(N_1, N_2) = \epsilon_p^a N_1 + \epsilon_e^b N_2 \quad (6)$$

where N_1 represents number of plastic cycles, N_2 number of elastic cycles.

Employing Coffin's interpretation of the strain at fracture ϵ_f to represent half the strain range of a quarter cycle fatigue excursion and equation (5),

$$C_p + C_e = (2\epsilon_f)^a / 4 + (0.9 \sigma_{ult} / E)^b 10^5 \quad (7)$$

Fracture will be proposed to occur when $D(N_1, N_2) = C_p + C_e \quad (8)$

$$\text{or } \epsilon_p^a N_1 + \epsilon_e^b N_2 = (2\epsilon_f)^a / 4 + (0.9 \sigma_{ult} / E)^b 10^5 \quad (9)$$

The constant C_e is many orders of magnitude smaller than C_p and can thus be neglected. This can best be illustrated by considering the exponent

THEORETICAL CONSIDERATIONS (Cont.)

values for SAE 4340 steel reported in reference [18] ; $a = 1.7$, $b = 10$.

Considering an ultimate tensile strength of 150,000 psi and ductility of 20%,

$$C_p = (2(0.2))^{1.7/4} = 0.0525, \text{ and } C_e = (0.9 (150000) / 30(10^6))^{10} 10^5 =$$

0.34×10^{-18} . For similar reasons, if N_1 is within several orders of magnitude comparable to N_2 , and ϵ_p is comparable to ϵ_e , the contribution of damage by elastic straining is negligible. This is generally the case when strain cycling plastically, so that equation (9) reduces to

$$\epsilon_p^a N = (2\epsilon_f)^a / 4 \quad (10)$$

There are several techniques proposed to handle the effect of mean strain.

Ohji, et al. [11], as a result of a linear damage theory expressed by the following equation,

$$\sum_{i=1}^k \epsilon_p^a N = (2\epsilon_f)^a / 4 \quad (11)$$

proposes equation (10) take the following form as a result of the mean strain

ϵ_m :

$$\epsilon_p^a N = (2\epsilon_f)^a / 4 - (2\epsilon_m)^a / 4 \quad (12)$$

Sachs, et al. [10] suggests the equation for mean strain is

THEORETICAL CONSIDERATIONS (Cont.)

$$\epsilon_p N^{1/2} = \epsilon_f - \epsilon_m \quad (13)$$

This equation assumes a value of $a = 2$. Re-arranging equation (13) and defining the exponent in the general form, a , results in

$$\epsilon_p^a N = (2 \epsilon_f - 2 \epsilon_m)^{a/4} \quad (14)$$

This expression mathematically implies that damage accumulates non-linearly as expressed by the following equation

$$\sum_{i=1}^k \epsilon_p N^{1/a} = (2 \epsilon_f - 2 \epsilon_m)^{a/4} \quad (15)$$

Manson [19] proposes the same expression as Sachs; however, he supports a linear-cumulative damage theory. Although there is a mathematical conflict indicated, physical interpretation of a shift of the stress-strain curve in a strain direction supports this latter hypothesis. This author subscribes to this hypothesis. Application to equation (5) (with the additional stipulation of no plastic strain cycling, which will be shown later as the case for the particular load mode selected for this study) results in the following expression.

$$\epsilon_e^b N = (2 \epsilon_f - 2 \epsilon_m)^{a/4} \quad (16)$$

For the case of several cyclic strain ranges about the same mean strain

THEORETICAL CONSIDERATIONS (Cont.)

value, ϵ_m , this becomes

$$\sum_{i=1}^k \epsilon_{ei}^b N_i = (2\epsilon_f - 2\epsilon_m)^2 / 4 \quad (17)$$

Defining N_i as the cyclic life at a cyclic strain range of ϵ_{ei} , equation (17) reduces to Miner's linear cumulative damage expression

$$\sum_{i=1}^k \eta_i / N_i = 1.0 \quad (18)$$

For the case of several different mean strain values, $\epsilon_m(1) \epsilon_m(2) \dots$

ϵ_{mj} , N_{ij} will be defined as the cyclic life at a cyclic strain range of ϵ_{ei} imposed on a mean strain value of ϵ_{mj} . For this case, fracture will assume to occur when

$$\sum_{i=1}^k \sum_{j=1}^l \eta_{ij} / N_{ij} = 1.0 \quad (19)$$

Biaxiality effects are accounted for by the effective plastic strain quantity, $\bar{\epsilon}_p$, first proposed by Dorn and Thompson [20] based on the von Mises (or Octahedral Shear Stress) theory.

$$\bar{\epsilon}_p = (2)^{1/2} \left((\epsilon_{p1} - \epsilon_{p2})^2 + (\epsilon_{p3} - \epsilon_{p1})^2 \right)^{1/2} / 3 \quad (20)$$

THEORETICAL CONSIDERATIONS (Cont.)

Equivalent stress is defined as

$$\bar{\sigma} = \left((\sigma_1 - \sigma_2)^2 + \sigma_2^2 + \sigma_1^2 \right)^{1/2} / (2)^{1/2} ; \sigma_3 = 0 \quad (21)$$

where $\epsilon_p \dots \epsilon_{p3}$, and σ_1, σ_2 are principal strains and stresses.

EXPERIMENTAL PHASE

The primary material selected for evaluation was SAE 4340 steel in the Rc 28-32 hardness range. This intermediate hardness was chosen as representing the asymptotic value to which hardened SAE 4340 steel strain softens, and annealed SAE 4340 steel strain hardens, as reported in reference [17] .

There was some limited additional work conducted with C355, a high precision cast aluminum alloy exhibiting a hardness of 80 BHN. The chemical composition of these alloys is contained in tables 1 and 2. The mechanical properties determined from 0.250-dia., 1.25-inch gage length tensile specimens are contained in tables 3 and 4 for the steel and aluminum alloys, respectively. Although the hardness range specified for the steel alloy was maintained, differences in the mechanical properties (and more critical, stress-strain relationships) warranted classification into three groups which are designated A, B, and C for this report.

The test vehicle employed in this study was a rotating disk which will be referred to as a rotor. Figure 1 is a photograph of the rotor, while figure 2 is a schematic presentation of the rotor. The rotors exhibited a

EXPERIMENTAL PHASE (Cont.)

6.3-inch OD and tapered hub with a test section thickness of 0.200 inch at a 2.15-inch radius. Notched rotors were also tested and displayed the same configuration with the addition of a 0.030 full radius circumferential notch machined on both sides of the rotor at the test section. The aluminum rotors were identical to the steel rotors in the disk area but contained 60 dummy blades reflected against 18 for the steel rotors.

The rotors were speed cycled in the spin pit facility shown in figure 3. This facility is composed of a pneumatically-driven three-inch OD drive turbine, a six-foot-diameter armour plated containment housing and associated oil mist bearing lubrication system, a vacuum pump for evacuating the pit during testing, and a control console to monitor speed cycling. Photographic equipment for permanent recording of burst modes is also available.

Figure 4 is a photograph of one of the steel rotors taken at the instant of burst (55,800 rpm). Strain was related to speed analytically, employing the methodology and analyses developed by Manson [21].

A summary of the pertinent formulation is reproduced in the appendix to provide an understanding of the basic approach. The technique incorporates the experimental determination of stress-to-strain relationships in the plastic range for the subject materials. This was determined from 12 SAE 4340 specimens and six C355 0.250-dia., 1.25-inch gage length,

EXPERIMENTAL PHASE (Cont.)

specimens that were removed from the hub sections of 18 rotors following fracture. The method presented in the appendix is based on von Mises' theory, which is sometimes referred to as the Deformation Theory, and is valid only if the loading path is such that the ratio of principal strain increments is constant throughout the straining period. This assumption appears to be sound, based on measurements taken by Waldren and Ward [22] on rotating disks at intervals in the loading cycle and the degree of success of Waldren, Percy and Mellow [23] in predicting disk burst speeds utilizing the theory. Care must be exercised, however, in the event the load is reversed, as the original stress-strain path will not be retraced. This is always the case when evaluating fatigue behavior of materials that have been exposed to plastic flow. This is considered in greater detail in the next topic, which presents strain-to-speed response for a rotor.

LOADING MODE STRAIN RESPONSE

Figure 5 is a schematic presentation of the strain response of the test rotor to speed cycling. The stress and strains can be considered equivalent values. It is recognized that the form of the equivalent stress and strain relationships preclude the possibility of negative values; nevertheless, equivalent residual stresses are plotted as compressive, when both radial and tangential components are negative for physical comprehension purposes.

LOADING MODE STRAIN RESPONSE (Cont.)

The plot depicts equivalent, total, plastic and elastic strains, and equivalent stress. Equivalent stress and equivalent plastic strain are direct consequences of the Deformation Theory and are expressed by

$$\bar{\sigma} = (\sigma_r^2 + \sigma_\theta^2 - \sigma_r \sigma_\theta)^{1/2} \quad (22)$$

$$\bar{\epsilon}_p = 2(\epsilon_{rp}^2 + \epsilon_{\theta p}^2 + \epsilon_{rp} \epsilon_{\theta p})^{1/2} / (3)^{1/2} \quad (23)$$

Total equivalent strain is defined through analogy by Manson [17] as

$$\epsilon_T = 2(\epsilon_{rT}^2 + \epsilon_{\theta T}^2 + \epsilon_{rT} \epsilon_{\theta T})^{1/2} / (3)^{1/2} \quad (24)$$

The expression resulting for equivalent elastic strain becomes

$$\bar{\epsilon}_e = 2(1+\mu) \bar{\sigma} / 3E \quad (25)$$

As the rotor is brought from zero speed to a maximum value, a strain excursion along line 0-0'-1 is generated. The respective strain excursion upon returning to zero speed is depicted as line 1-2. Point 2 represents the residual stress and strain incurred during this first speed cycle. The residual stresses and strains are readily obtained analytically, employing an elastic solution where initial strains are those values existing at point 1. The yield point is noted to have increased to a minimum value equal to that which occurred at maximum speed from the previous loading. This

LOADING MODE STRAIN RESPONSE (Cont.)

behavior is the so-called "Bauschinger Effect" and was supported for the two materials under investigation by examining strain-to-load response when cycling several uniaxial tensile specimens removed from fractured test rotors. Upon re-loading, the strain response is indicated by line 2-3 for the same maximum speed. The cyclic strain range is shown in the figure as ϵ_e and is equal to $2(1 + \mu) \Delta \sigma / 3E$ where

$$\Delta \bar{\sigma} = \left((\Delta \sigma_r)^2 + (\Delta \sigma_\theta)^2 - (\Delta \sigma_r)(\Delta \sigma_\theta) \right)^{1/2} \quad (26)$$

It should be emphasized that this model represents the strain response due to speed, i.e., speed is the independent or test input variable and strain the resultant or dependent value. The majority of work done previously has been strain-monitored in that the test specimen was physically forced to cycle over a constant strain interval. This resulted in a varying load input; increasing for strain-hardening materials and decreasing for strain-softening materials. As most structures are low-cycle fatigue-tested through load excursions, it was elected to monitor the testing reported here through centrifugal load or speed. Speed cycling of rotors is seen to reduce to elastically cycling a material that has experienced a reduction in ductility. Equations (16) and (17) proposed to define life under conditions of single and multiple strain ranges are rewritten as follows to include biaxial effects.

$$\bar{\epsilon}_e^b N = (2 \bar{\epsilon}_f - 2 \bar{\epsilon}_m)^a / 4 \quad (27)$$

LOADING MODE STRAIN RESPONSE (Cont.)

$$\sum_{i=1}^k \bar{\epsilon}_{e_i}^b \eta_i = (2\bar{\epsilon}_f - 2\bar{\epsilon}_m)^a / 4 \quad (28)$$

where $\bar{\epsilon}_e$ is designated cyclic elastic equivalent strain and defined by equation (25), and $\bar{\epsilon}_f$ and $\bar{\epsilon}_m$ are designated total equivalent strain values expressed by equations (23) and (24), respectively.

TEST LOADING MODES

There were three test phases employed in this study that can be classified according to the associated loading mode. Defining load ratio as $R_n = N_{\min}/N_{\max}$ where N_{\min} and N_{\max} represent minimum and maximum speeds of a cyclic speed range, the first phase consisted of running in an $R_n = 0$ mode. Physically, this represents stop-start operation of a rotative structure. The second phase consisted of running in an $R_n = R$ mode where $0 < R < 1.0$. This represents speed excursions about a normal operating value. The third phase consisted of speed cycling at various successive R_n modes to evaluate cumulative damage effects. Figure 6 is a schematic plot of strain response associated with these loading modes. SAE 4340 material classified into groups A, B, and C in table 3, respectively, were evaluated in the three test phases; C355 was tested in the first phase, $R = 0$, only.

TEST RESULTS

Figure 7 contains true stress-true strain diagrams for the two materials and represents the average values obtained from a minimum sample size of three specimens removed from rotors per group. Figures 8 and 9 present the cyclic-elastic strain distribution and plastic strain distribution, respectively, for the polished rotor. Figures 10 and 11 depict the counterparts for the notched rotor. The biaxial strain ratios for the cyclic strains at the test sections of the rotors are 0.42 and 0.32 for the polished and notched rotors, respectively. It should be noted that the ratios for the plastic or mean strains are less than 0.1 at the test section. The mean strains can be considered uniaxial, although biaxial effects were carried along throughout the analytical phases of this investigation.

Figure 12 shows the relationship between equivalent plastic or mean strain with speed and equivalent cyclic elastic strain with speed. These strain values are plotted in dimensionless form, referring to the corresponding values at fracture. The reference for the cyclic strain should be interpreted as the cyclic equivalent strain excursion that would have been realized upon unloading from the speed of fracture if fracture had not occurred.

TEST RESULTS (Cont.)

The test objectives were to ascertain, accounting for biaxiality through von Mises' theory of combined stresses and strains under fatigue loading, if

1. an exponential relationship existed between cyclic life and cyclic strain employing this combined strain theory,
2. the exponent of strain-life dependency differed for elastic and plastic straining,
3. mean strain could be accounted for through a linear cumulative damage theory, considering the elastic and plastic straining, and if
4. notching appreciably affected low cycle fatigue behavior as determined from smooth or polished geometries.

Table 5 contains the results of single cyclic strain range tests for both polished and notched SAE 4340 material. The results for the C355 material are tabulated in table 6.

An examination of equation (28) reveals if mean strain is maintained constant a plot of $\bar{\epsilon}_e$, cyclic equivalent elastic strain, versus N (cyclic life) on a log-log coordinate system results in a straight line, the geometric slope having the value $1/b$. Conversely, if cyclic strain is constant, a plot of $\epsilon_f - \epsilon_m$, which will be defined as "available strain" versus N , will also result in a straight line with a geometric slope of $1/a$.

TEST RESULTS (Cont.)

Phase I testing, $R_n = 0$, resulted in essentially constant cyclic strain testing about different mean strain values. Thus, it can be considered to represent the cited converse case. Phase II testing, $R_n = R$, represents the former case when mean strain was maintained constant. As the testing evaluated this behavior at several mean strain values, data of constant cyclic strain nature was also obtained. Figure 13 is a plot of cyclic equivalent strain versus life for polished and notched SAE 4340. The corresponding exponents, "b", are tabulated in table 7. Figure 14 and figure 15 are plots of $\bar{\epsilon}_f - \bar{\epsilon}_m$ versus life for polished and notched SAE 4340 material, respectively. It should be noted that although the testing associated with the last two figures is considered constant cyclic strain, cyclic strain values $\bar{\epsilon}_e$ deviated from an average value up to 10%. Because small differences in $\bar{\epsilon}_e$ bring about large changes in $\bar{\epsilon}_e^b$, an iteration process based on the experimental value of "b" (previously determined) and equation (27) was conducted to correct the quantity $\bar{\epsilon}_f - \bar{\epsilon}_m$ to the average cyclic strain value. Figure 16 is a plot of $\bar{\epsilon}_f - \bar{\epsilon}_m$ versus N for polished and notched aluminum. The values represent uncorrected values, because only the $R_n = 0$ loading mode was evaluated for this material. The resulting values of "a" are also contained in table 7.

The average value of "b" obtained for the polished SAE 4340 of 9.15 agrees fairly well with the value of 9.61 obtained by Manson [17] for hardened

TEST RESULTS (Cont.)

SAE 4340 material. The corresponding value of "a" determined by Manson's work was 1.7 reflected against a value of 3.25 determined from this author's work. The generally accepted value for this quantity based on the results of Coffin and Tavernelli is 2.0; however, for specific material use it is recommended that this exponent be determined experimentally. Notching was seen to result in a somewhat lower value for both "a" and "b". This is consistent with the classical behavior of notched materials in which higher fatigue strengths than the polished configuration are realized in the low cycle fatigue operating regime but with greater strength-to-life gradients. The effect of notching on the aluminum alloy is seen to be more significant than on the steel, although, the average of the two configurations is approximately the same as the corresponding one for steel.

Table 8 contains the results of the cumulative damage phase of the investigation for both polished and notched rotors. The three loading modes presented schematically in figure 6 were employed in this study. In this third mode, it is noted that the maximum cyclic strain point for the second strain range lies below the transition from elastic to plastic behavior. Considering essentially the same available strain quantity, $\epsilon_f - \epsilon_m$, to apply to both cyclic strain values as indicated in the figure, results in much greater life than that predicted by a linear damage theory. The implication is that it is not only the strain range that dictates the amount

TEST RESULTS (Cont.)

accumulated damage, but also the maximum strain associated with each cycle. If this is less than the previous maximum value, damage rate decreases in excess of that indicated by ϵ^b . An equivalency that suggested itself was translating the stress-strain curve along the strain axis for this second strain range such that the maximum stress or strain point laid upon it, indicating onset of plastic flow. This would have the effect of increasing the $\epsilon_f - \epsilon_m$ value by the amount of strain associated with the translation. This technique was employed to obtain the N values shown in the table for this type of loading sequence.

The average $\sum n/N$ for the polished rotors was 0.99 with a low of 0.52 and high of 1.55. The average $\sum n/N$ for the notched rotors was 1.44 with a low of 0.78 and high of 3.06.

Figure 17 is a presentation of a fractographic investigation conducted on several of the test rotors following fracture. Figures 17a and 17b represent the C-355 material. Figures 17c and 17d represent the SAE 4340 alloy. As macroscopic evaluation of a fractured surface operating in the low cycle fatigue regime does not always result in an explicit definition of fracture mode, fractographic techniques were also employed in the post-test investigation.

TEST RESULTS (Cont.)

A two-stage platinum -carbon tape replication technique was employed. The resulting electron fractographs represent a 12,500-power magnification. Directing attention toward the aluminum, the edge locations are seen to exhibit a relatively flat topography and contain classical fatigue striations. The centers of the fracture surfaces are rather irregular. In fact, they are non-uniformly irregular typical of the varying grain sizes associated with a casting. The fracture mode associated with this appearance is static tensile and shear overload, resulting from a loss in load-supporting area. The life relationships expressed mathematically in this study represent a damage period that includes crack initiation and propagation to the extent that load-carrying capacity is exhausted due to the loss in area. The corresponding figures for steel display the same gross topographic dissimilarities. The center sections, however, exhibit a more uniform "dimpled" appearance indicating a grain structure more typical of forgings. Two sets of markings orthogonal to each other are seen in figure 17d. The horizontal markings in this figure are fatigue striations and are normal to the advancing crack direction. The vertical markings are "river" markings associated with differences in the crystal levels with respect to the crack plane. This fractography work confirms the existence of a fatigue-initiated mode of fracture with the fracture sequence being fatigue crack initiation, fatigue crack propagation, and tensile overload.

CONCLUSIONS

The following conclusions have been drawn, based on the results of this study primarily considering the SAE 4340 material.

1. Biaxial effects can be accounted for by using the von Mises theory of combined stresses and strains.
2. A linear damage theory applied to both elastic and plastic equivalent strains appears reasonable, based on the accumulated damage test results varying both mean strain and cyclic strain.
3. An exponential relationship exists between strain and cyclic life. The exponent expressing this dependency was approximately 9.2 for elastic strain and 3.2 for plastic strain.
4. Notching does not significantly alter the linear damage theory. The associated strain life power coefficients are reduced to 7.8 for elastic strain and 3.1 for plastic strain.
5. Limited testing of the cast aluminum alloy C355-T61 indicated that its behavior is similar to that of the tested steel.

The support of this study by U.S. Army Research Office-Durham is gratefully acknowledged.

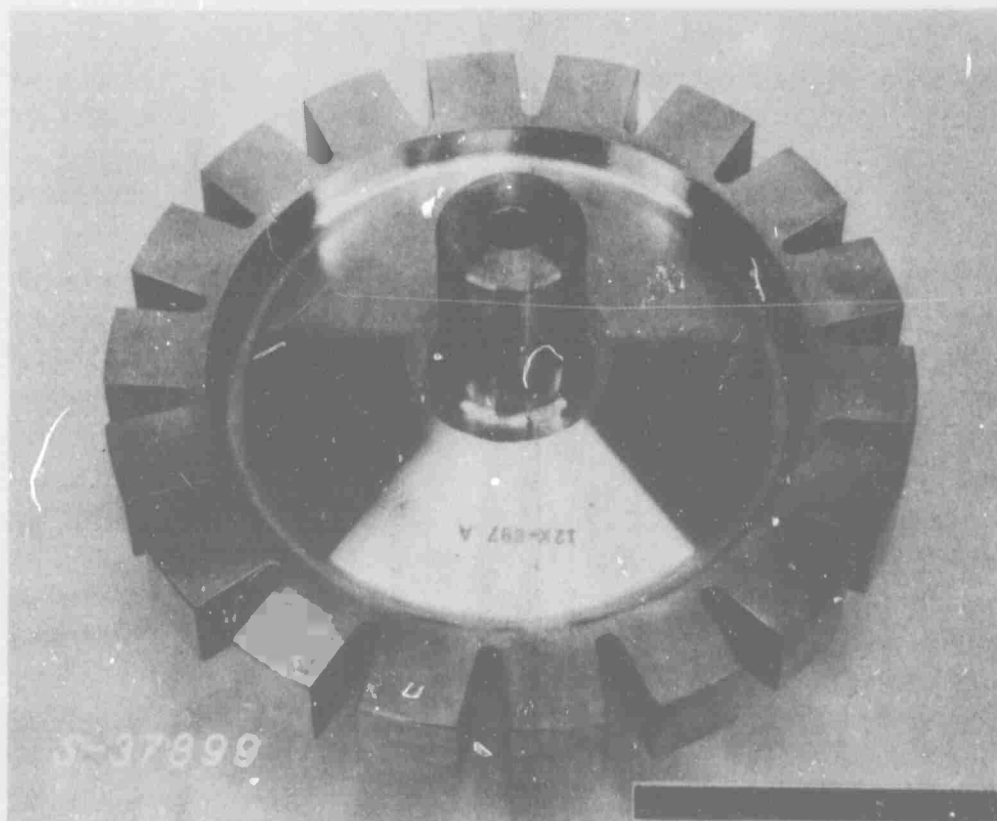
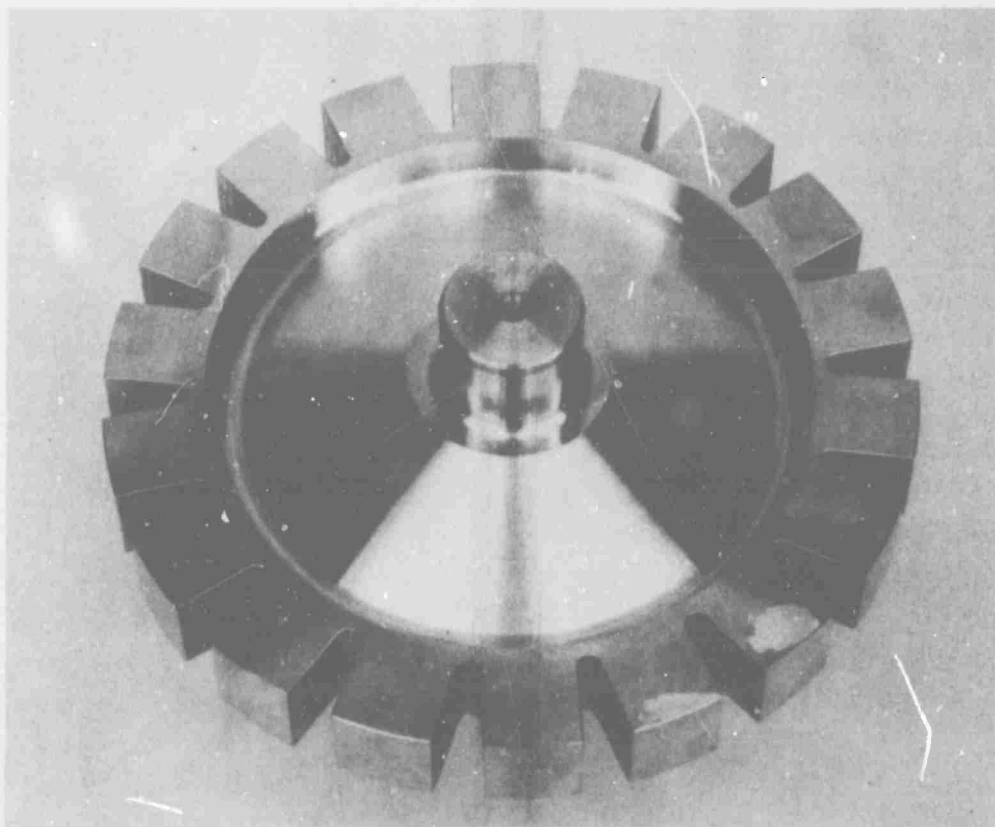


FIGURE 1. SAE 4340 TEST ROTOR

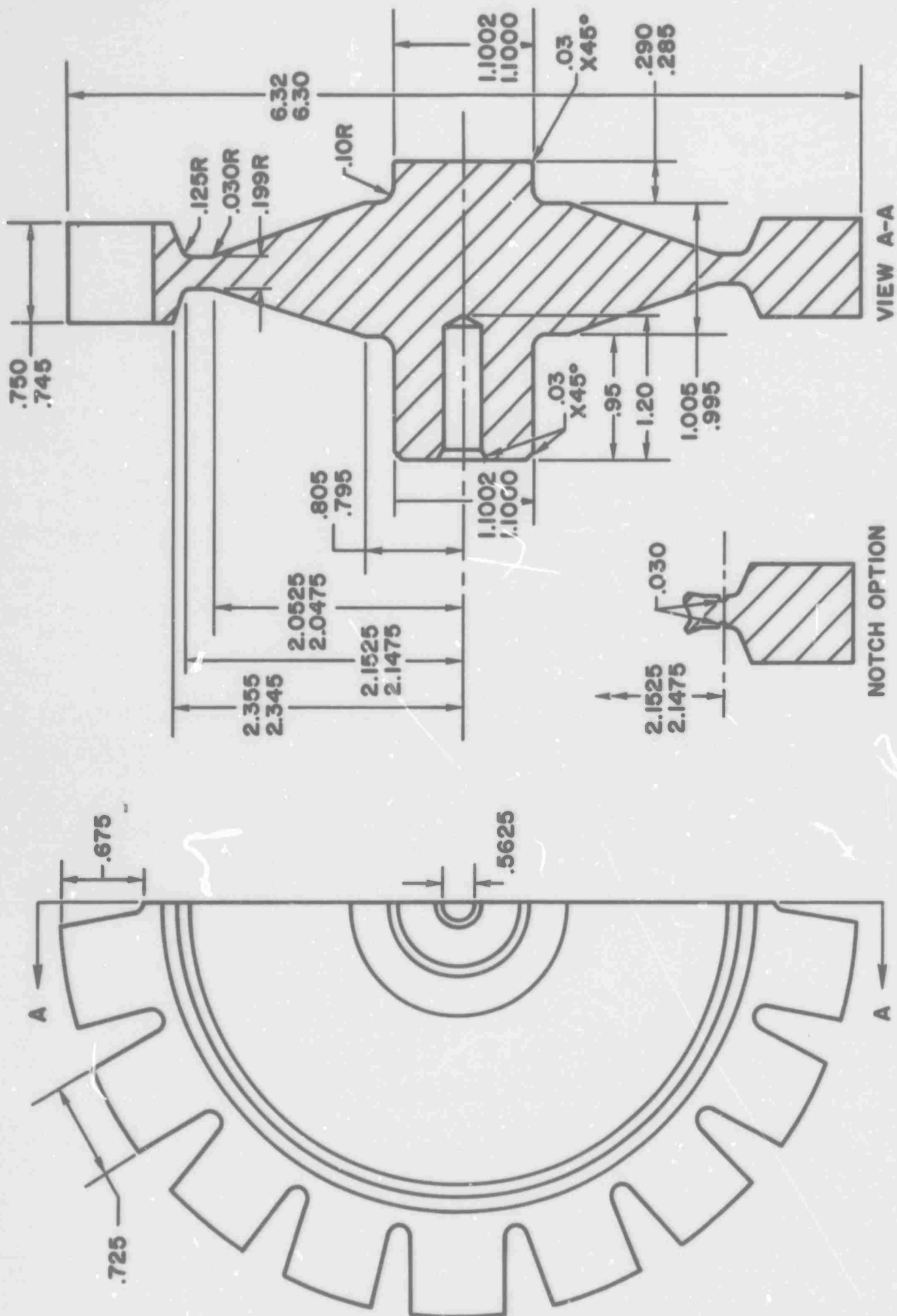


FIGURE 2. SCHEMATIC PRESENTATION OF TEST ROTOR

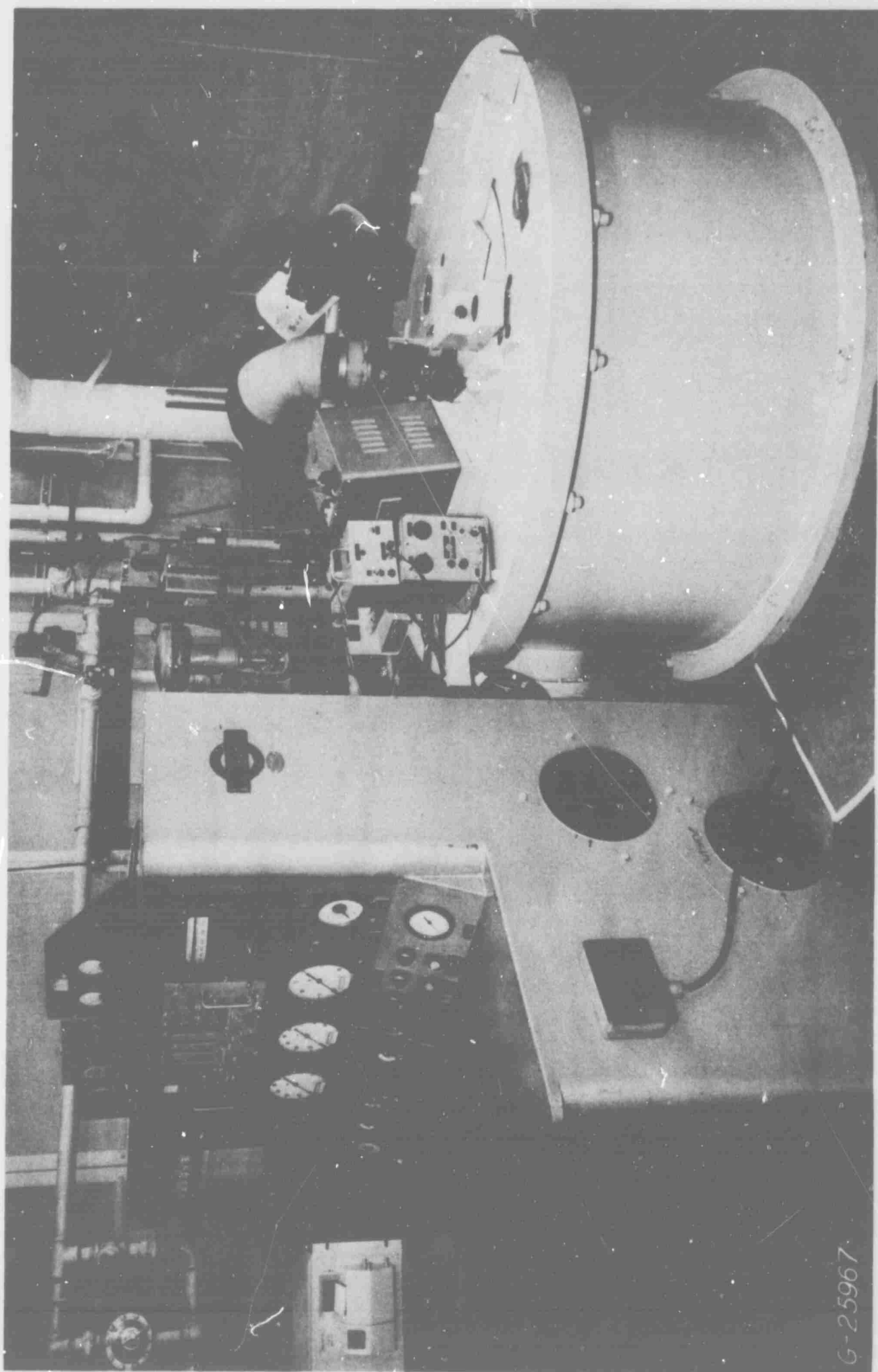


FIGURE 3. TEST FACILITY

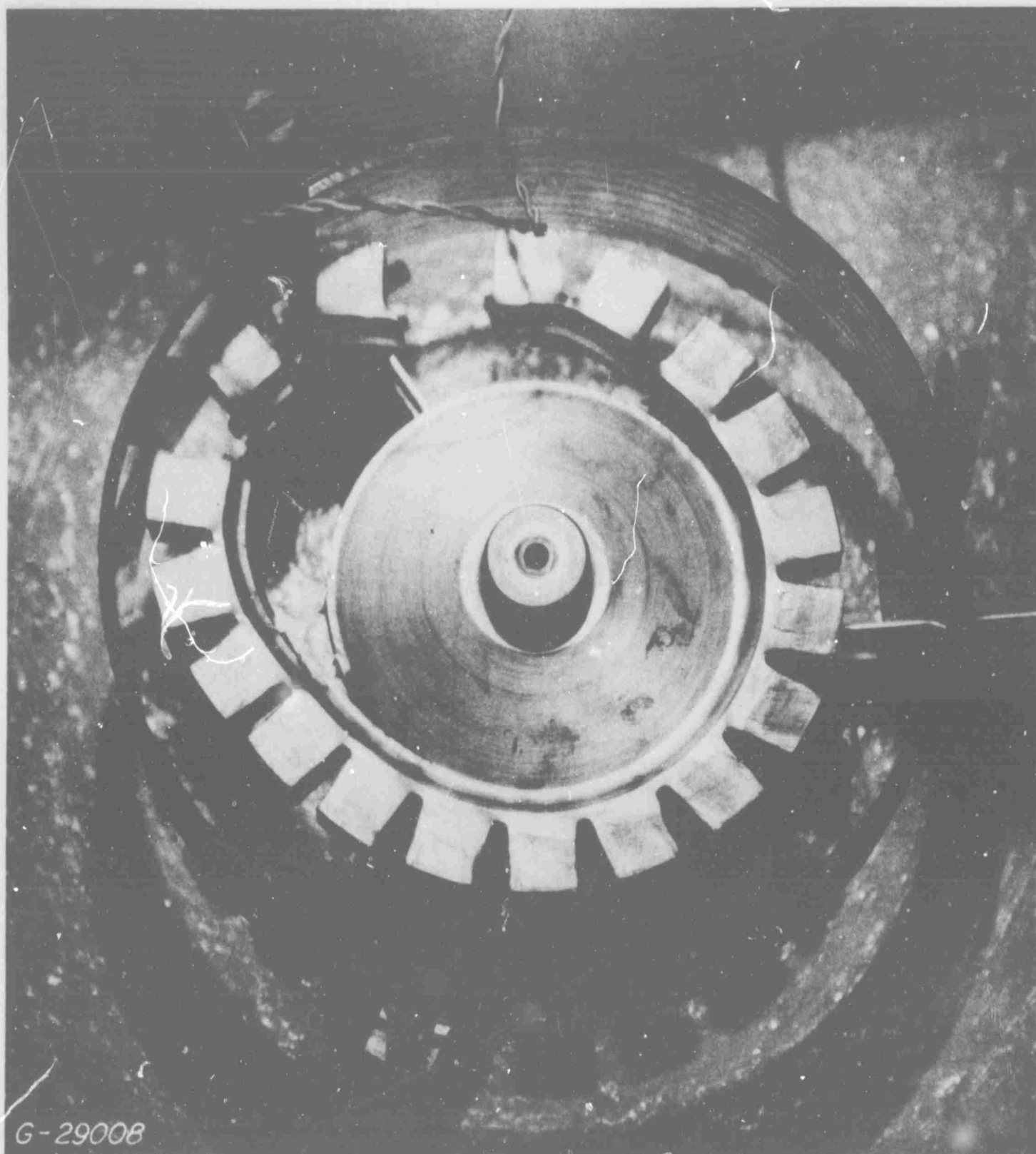


FIGURE 4. TEST ROTOR AT INSTANT OF BURST $N = 55,800$ RPM

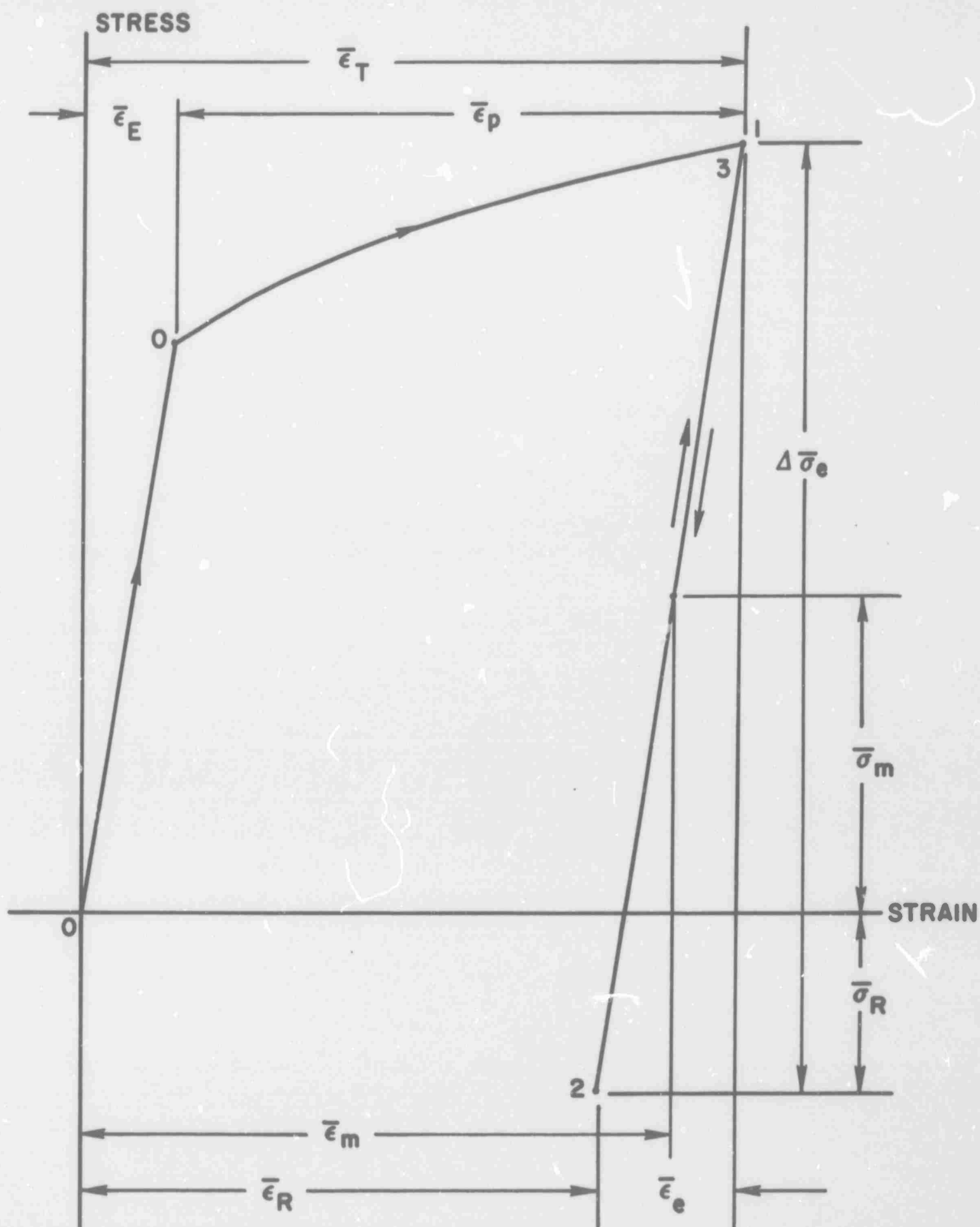


FIGURE 5. STRESS-STRAIN RESPONSE TO SPEED CYCLING

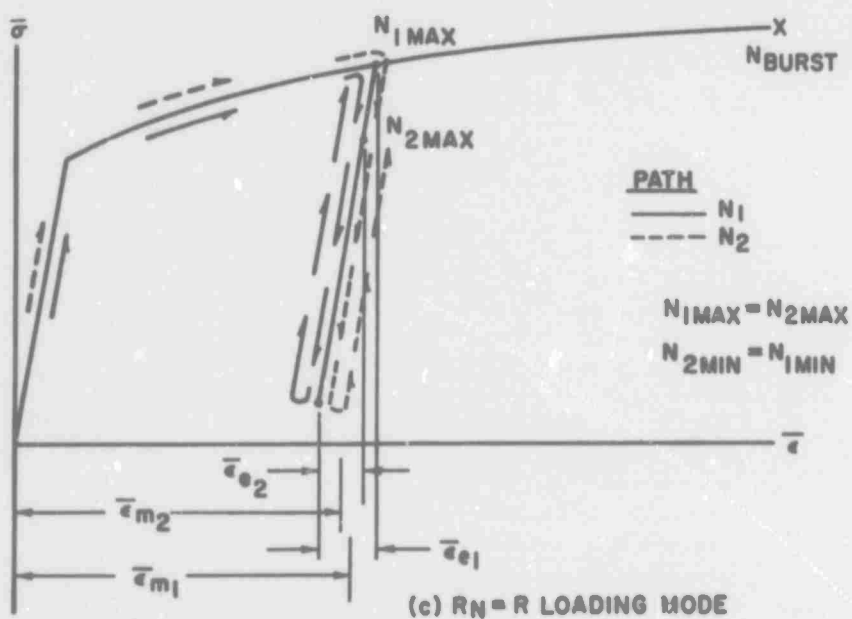
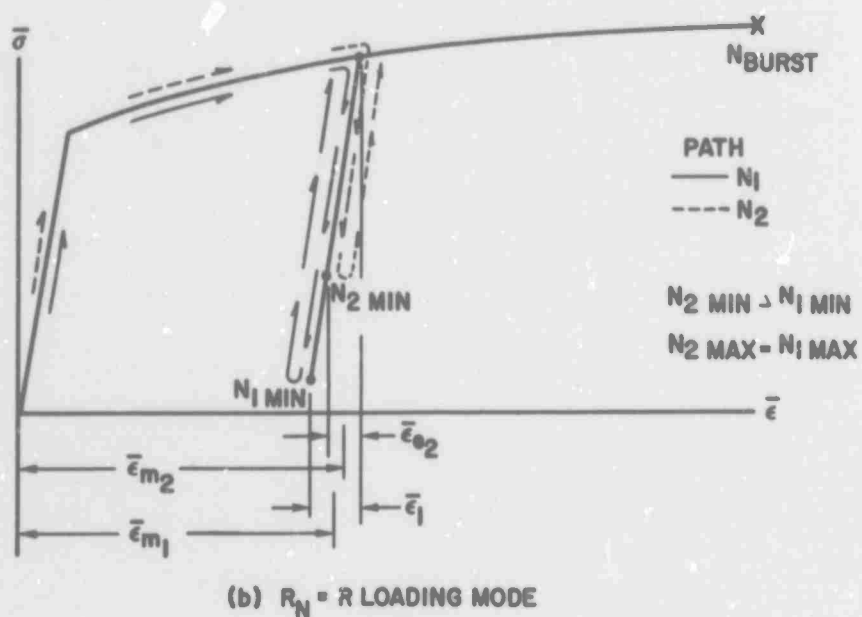
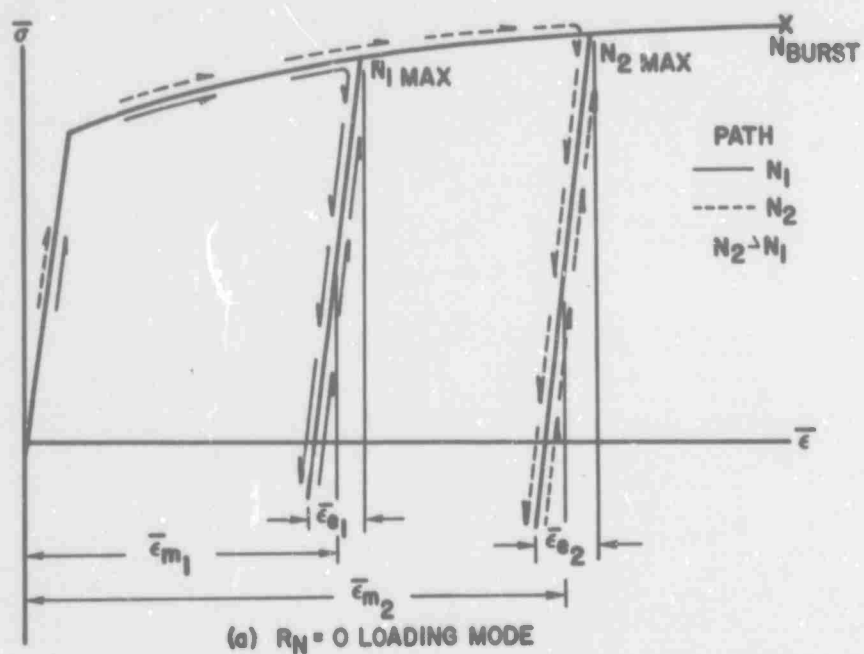


FIGURE 6. STRESS-STRAIN - LOAD RESPONSE

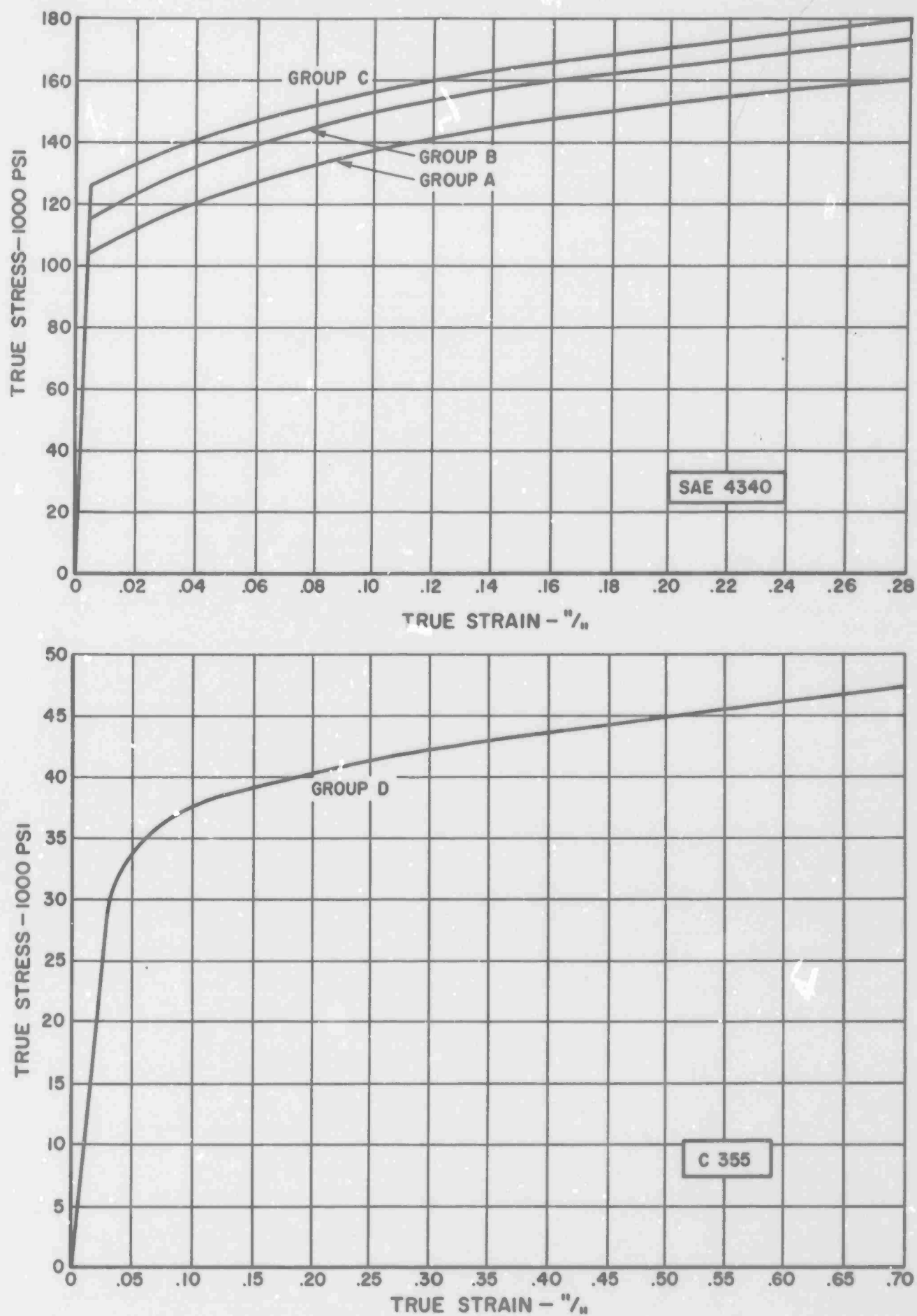


FIGURE 7. UNIAXIAL STRESS-STRAIN BEHAVIOR FOR SPECIMENS REMOVED FROM TEST ROTORS

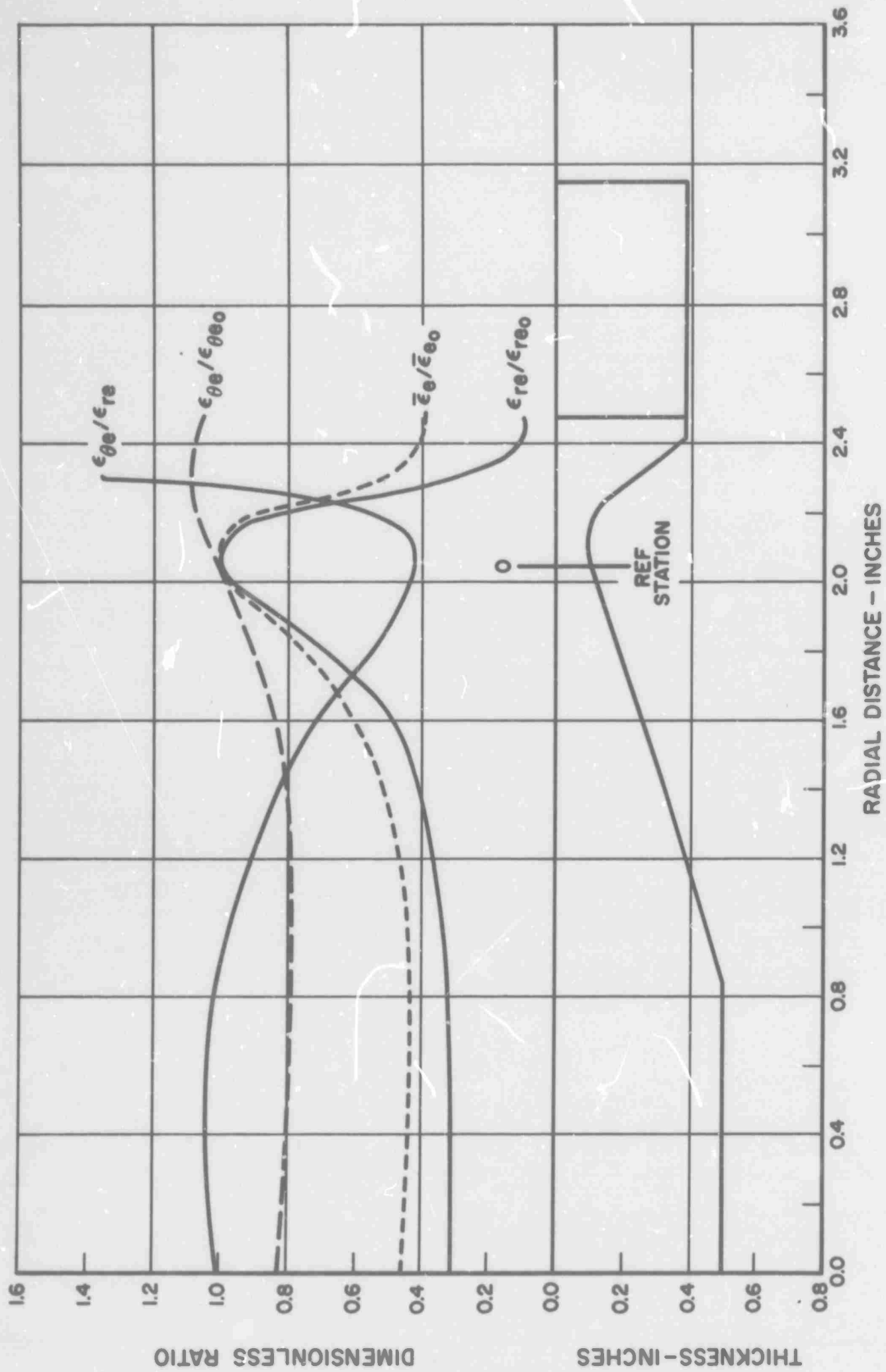


FIGURE 8. UNNOTCHED TEST ROTOR CYCLIC ELASTIC STRAIN DISTRIBUTION

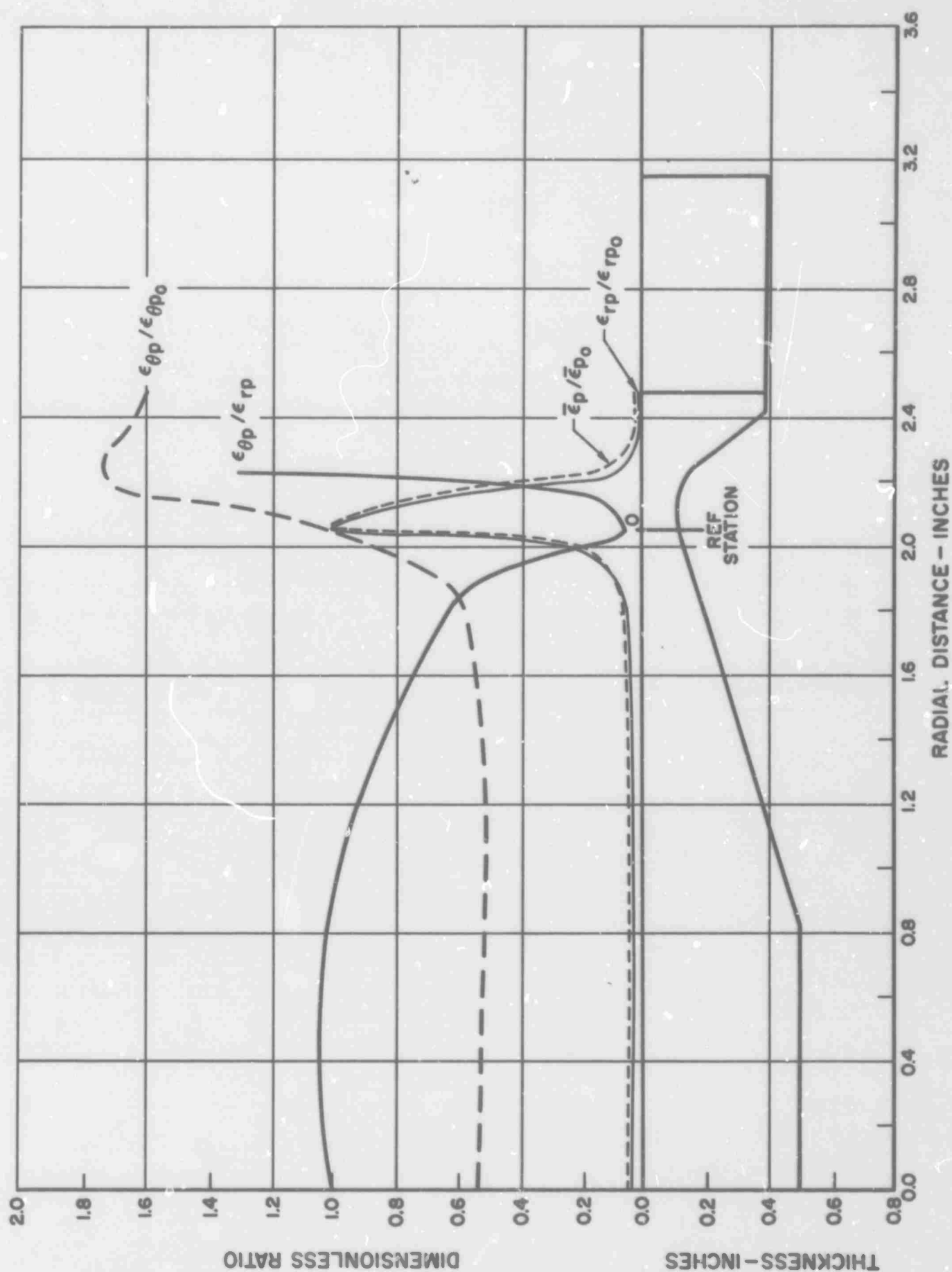


FIGURE 9. UNNOTCHED TEST ROTOR TYPICAL PLASTIC STRAIN DISTRIBUTION

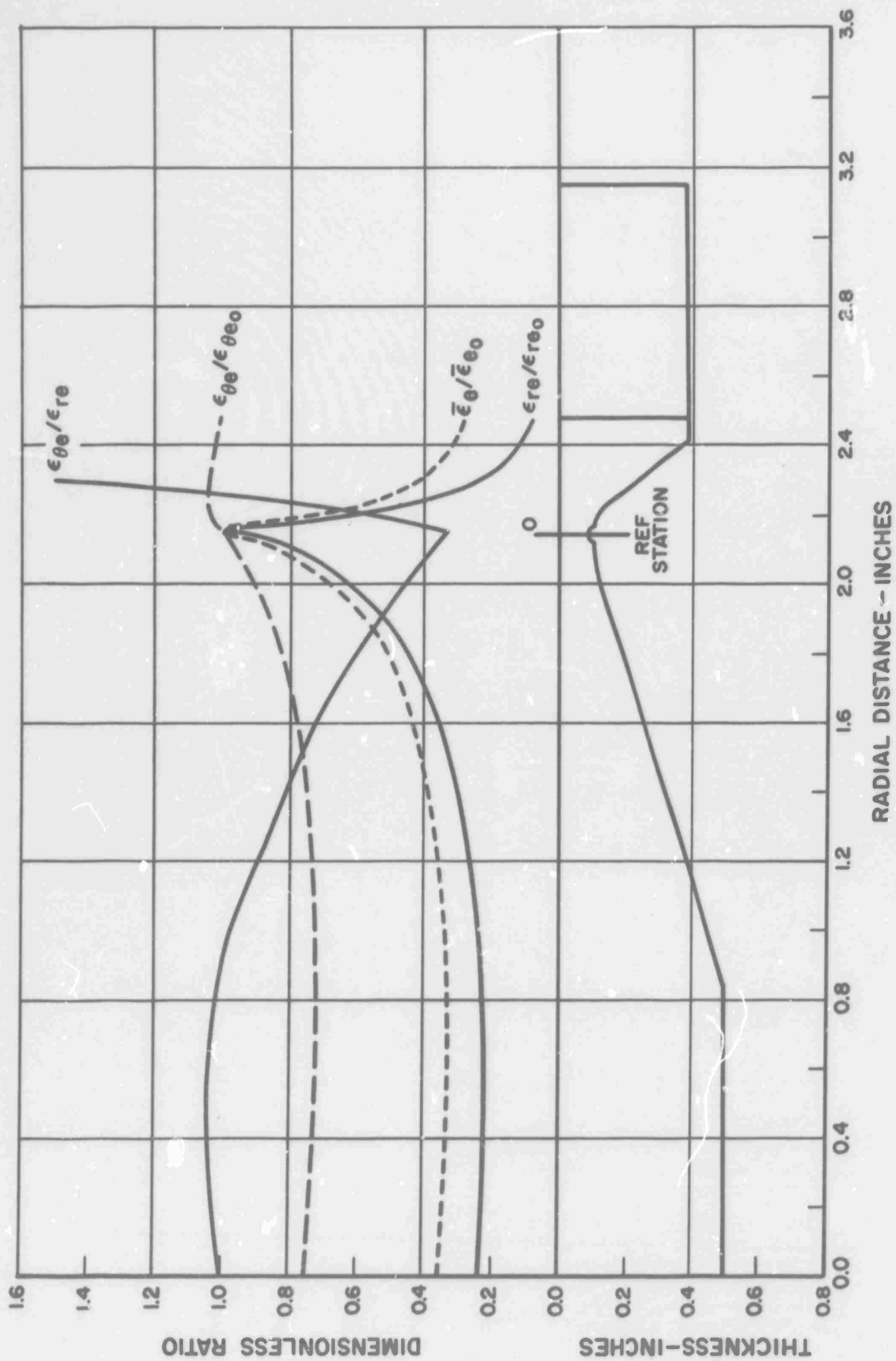


FIGURE 10. NOTCHED TEST ROTOR CYCLIC
ELASTIC STRAIN DISTRIBUTION

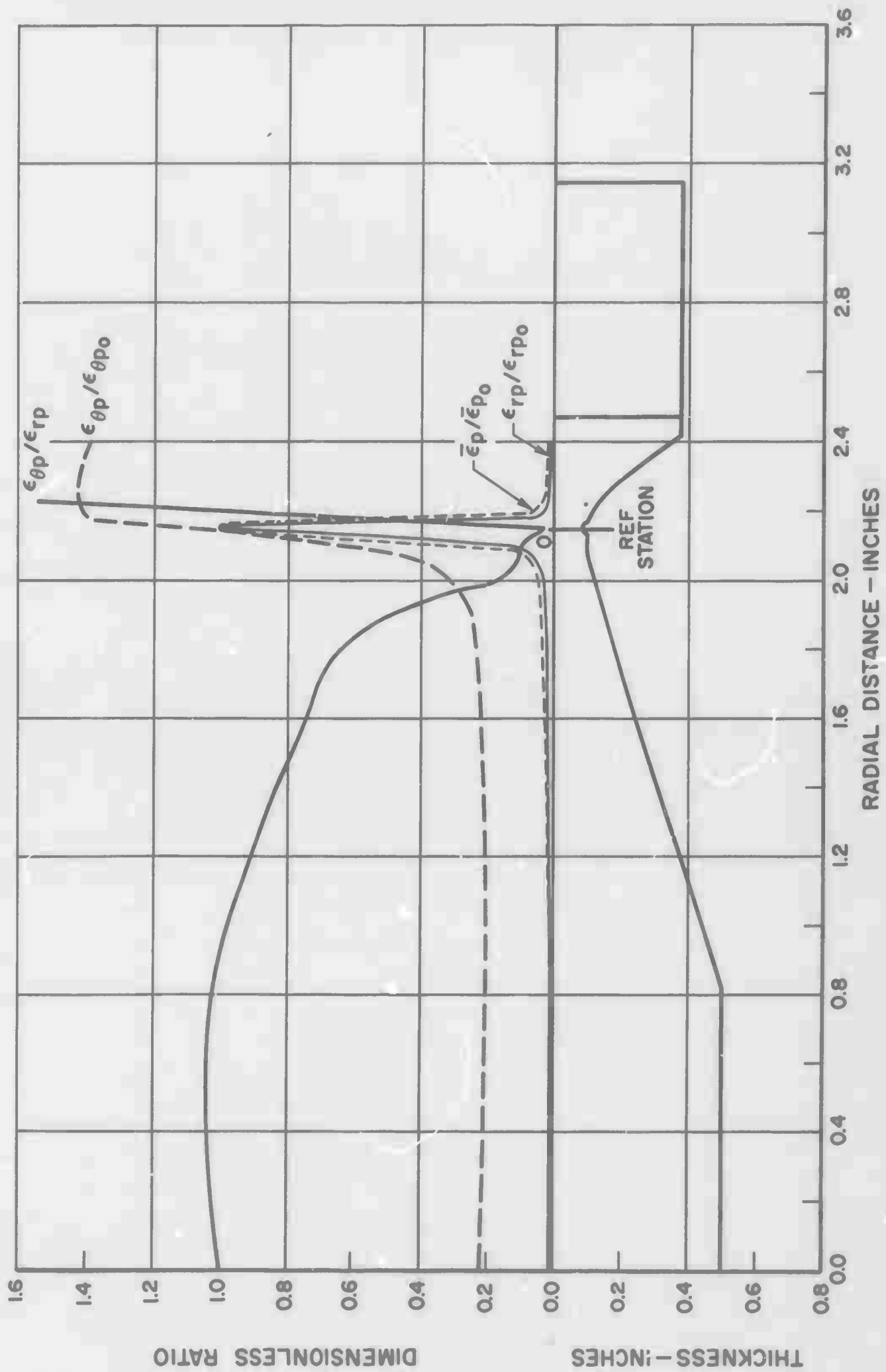


FIGURE 11. NOTCHED TEST ROTOR TYPICAL PLASTIC STRAIN DISTRIBUTION

MATERIAL	GROUP	SURFACE CONDITION	BURST SPEED RPM	EQUIVALENT STRAIN - $\mu"/\text{in}$	
				$\bar{\epsilon}_{pf}$	$\bar{\epsilon}_{ef}$
SAE 4340	A	POLISHED	55800	297000	5440
		NOTCHED	51000	428000	5870
	B	POLISHED	55750	232000	5620
		NOTCHED	53000	420000	6300
	C	POLISHED	57700	198000	5690
		NOTCHED	52600	293000	6120
C 355	D	POLISHED	58600	69700	4420
		NOTCHED	51500	83800	4550

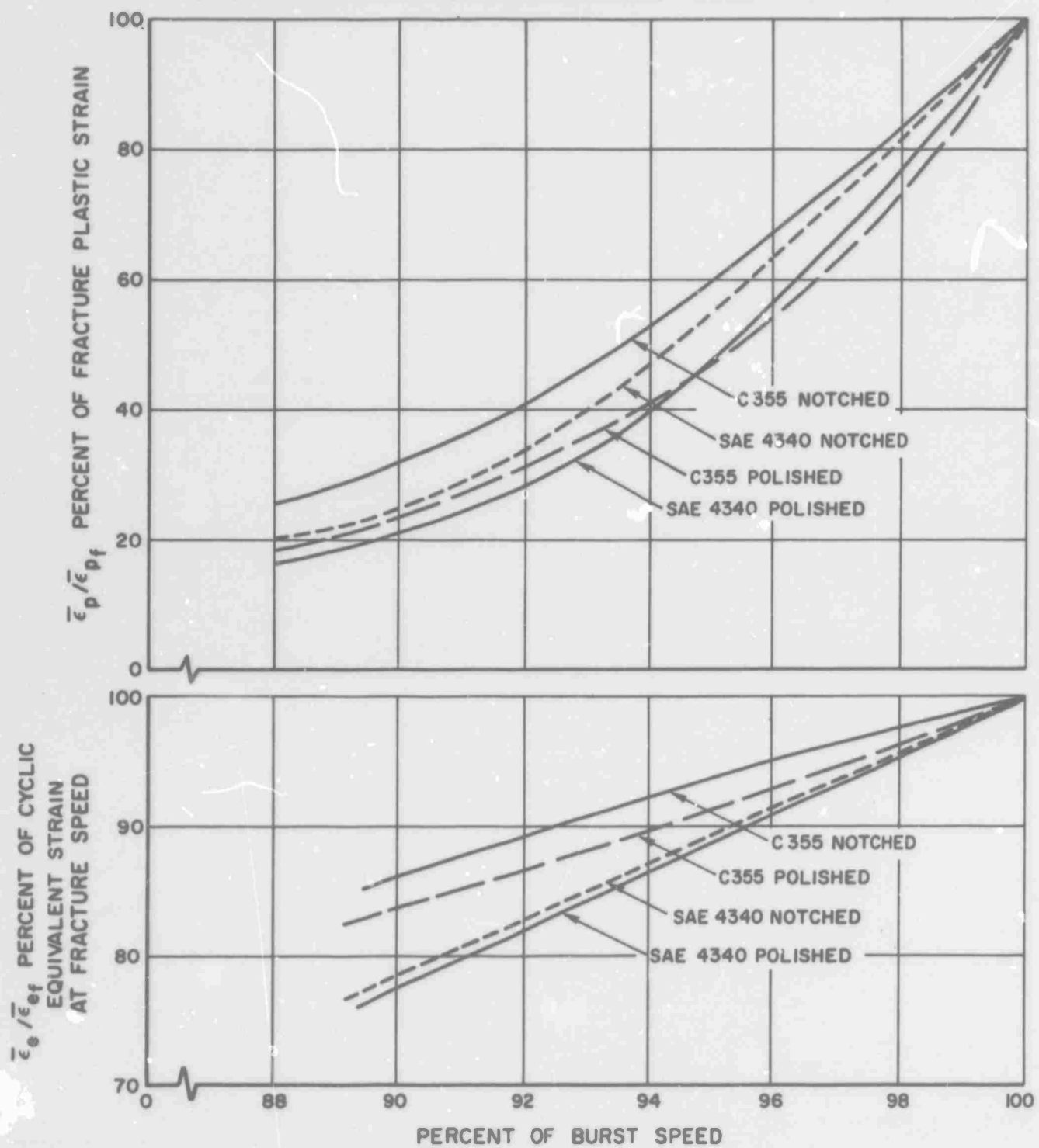


FIGURE 12. EQUIVALENT STRAIN VS SPEED AT TEST SECTION

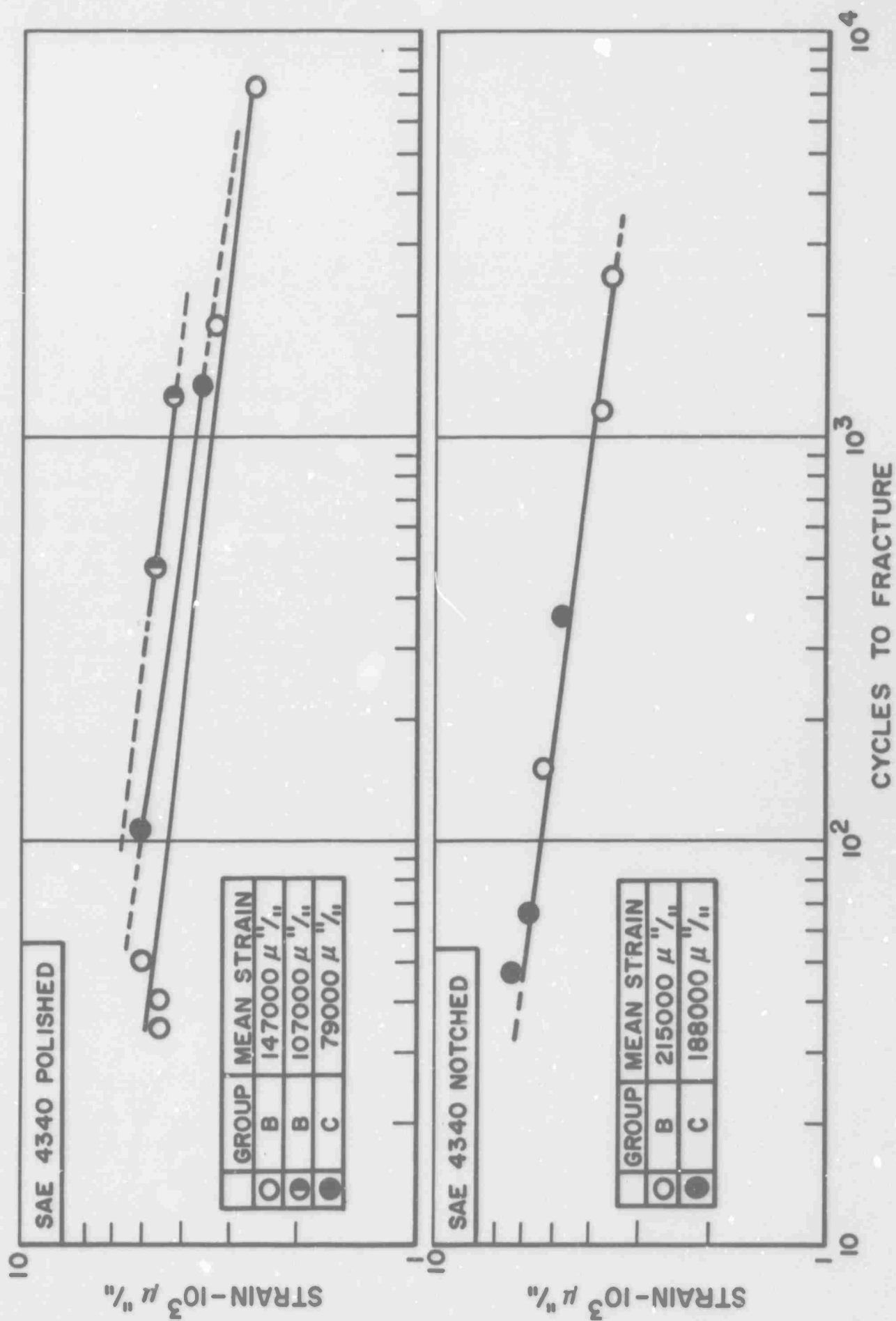


FIGURE 13. CYCLIC EQUIVALENT STRAIN VS
CYCLES TO FRACTURE

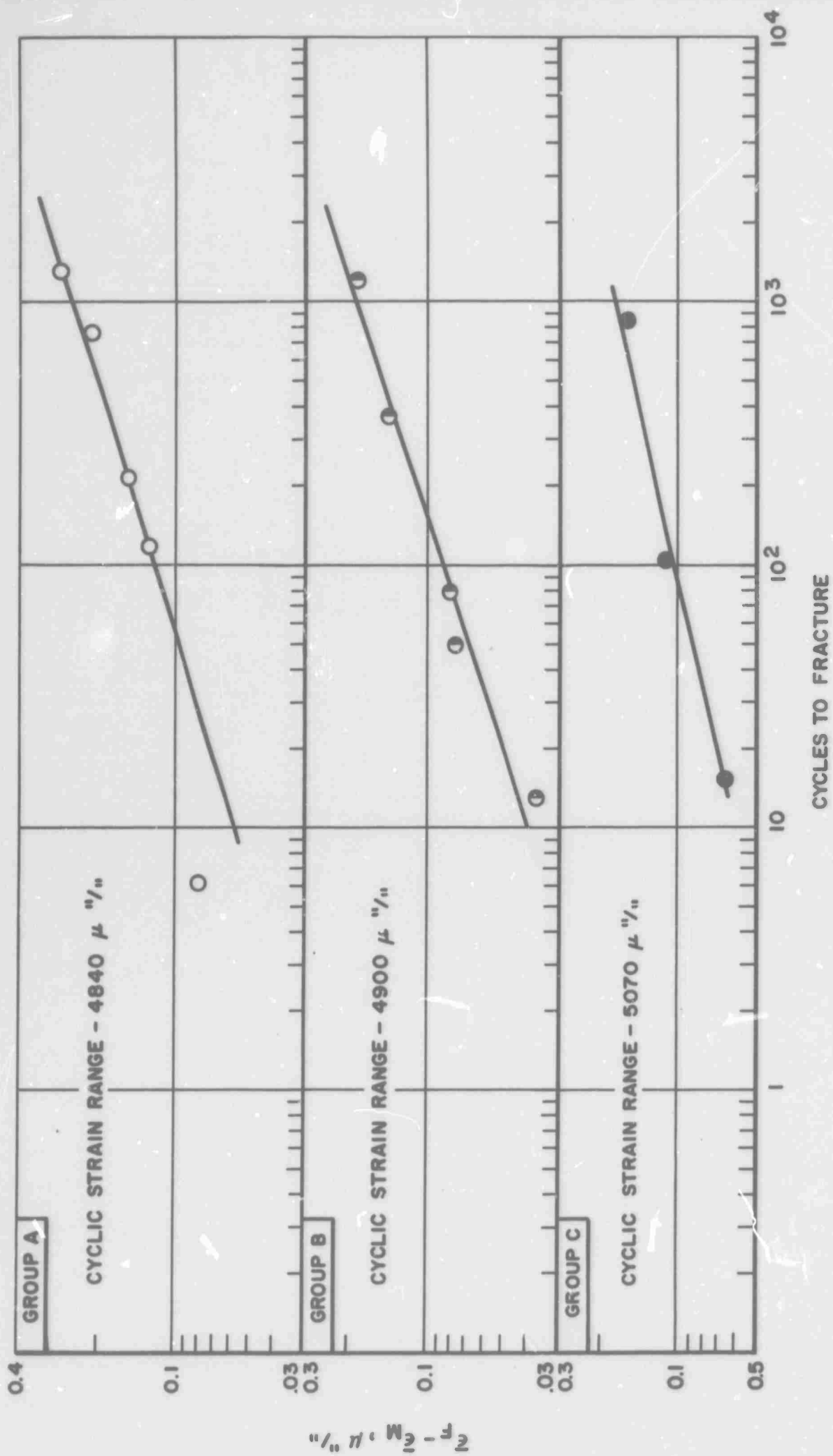


FIGURE 14. AVAILABLE STRAIN VS CYCLES TO FRACTURE - SAE 4340 POLISHED

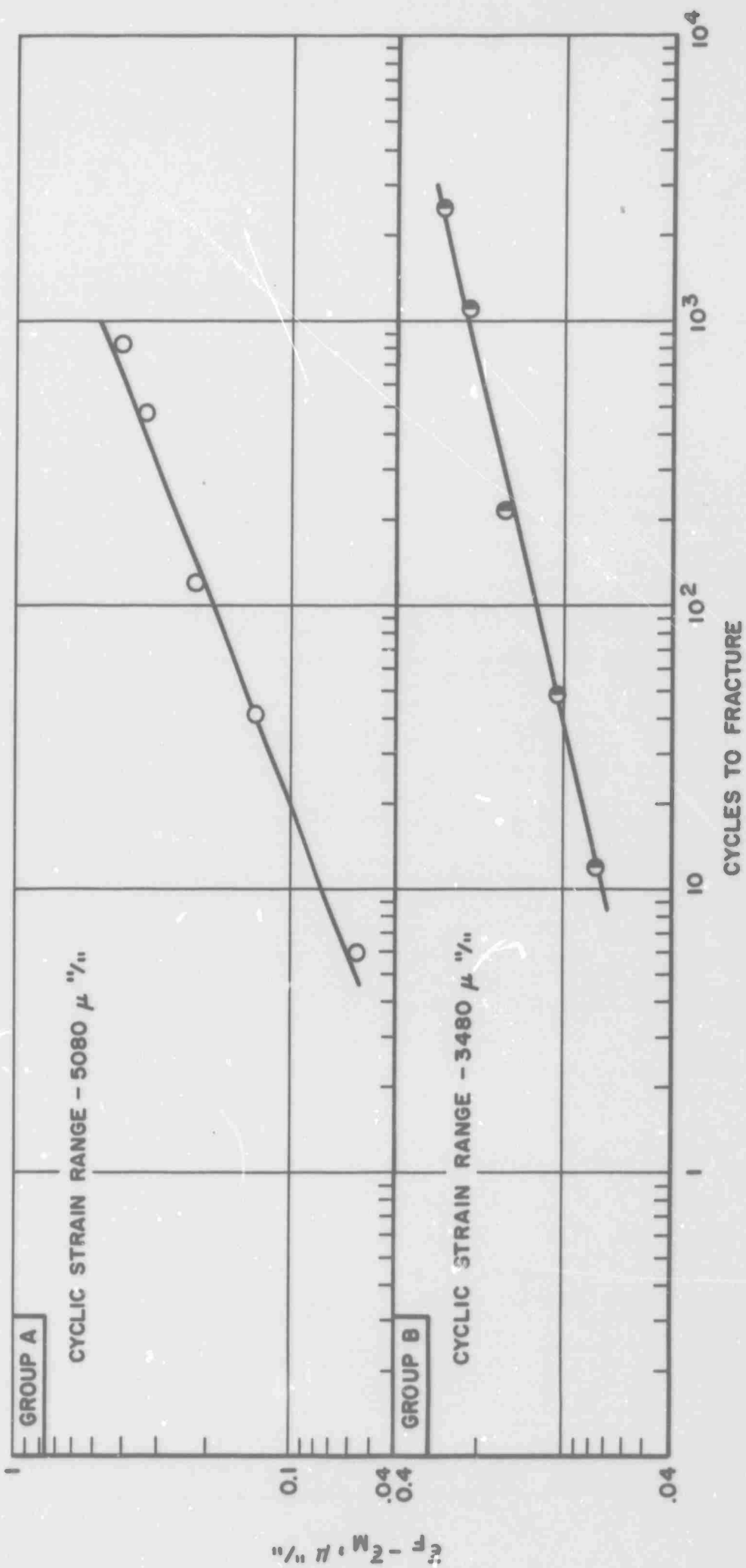


FIGURE 15. AVAILABLE STRAIN VS CYCLES TO FRACTURE - SAE 4340 NOTCHED

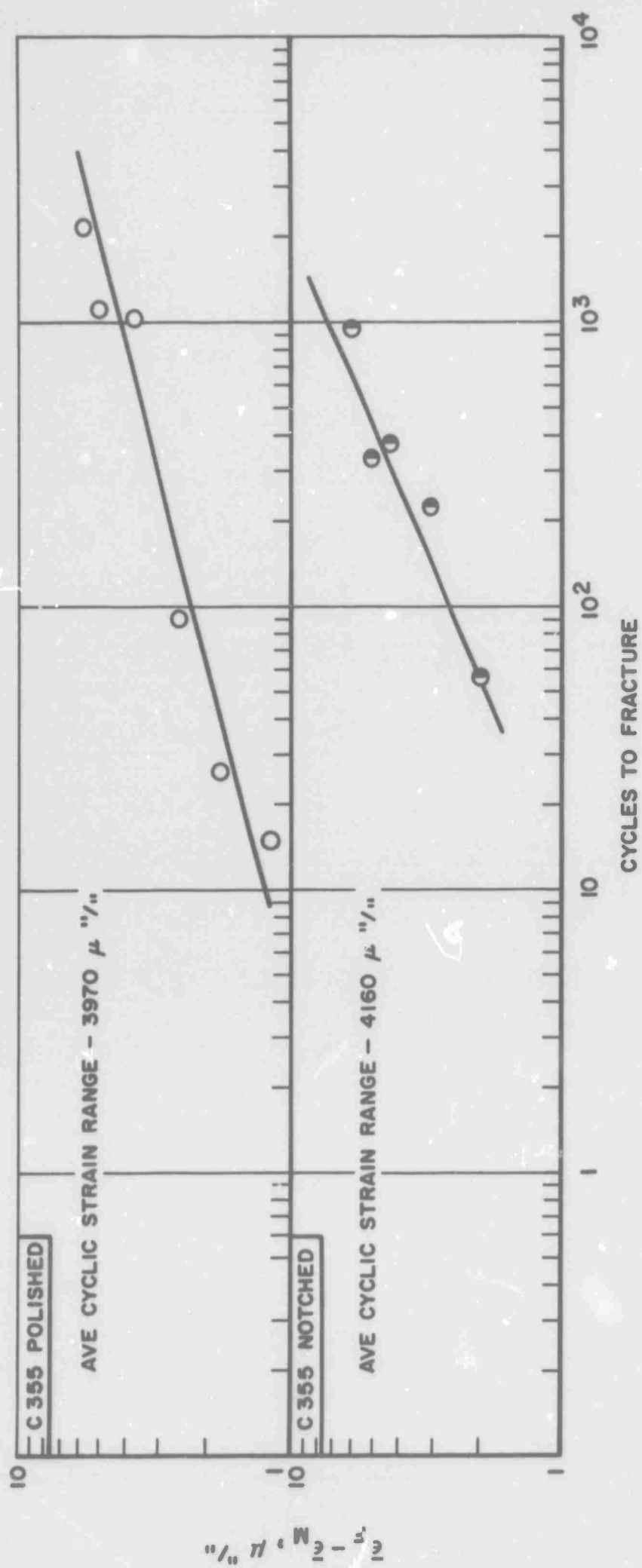


FIGURE 16. AVAILABLE STRAIN VS CYCLES TO FRACTURE - C 355

EDGE OF
FRACTURE
SURFACE



CENTER OF
FRACTURE
SURFACE

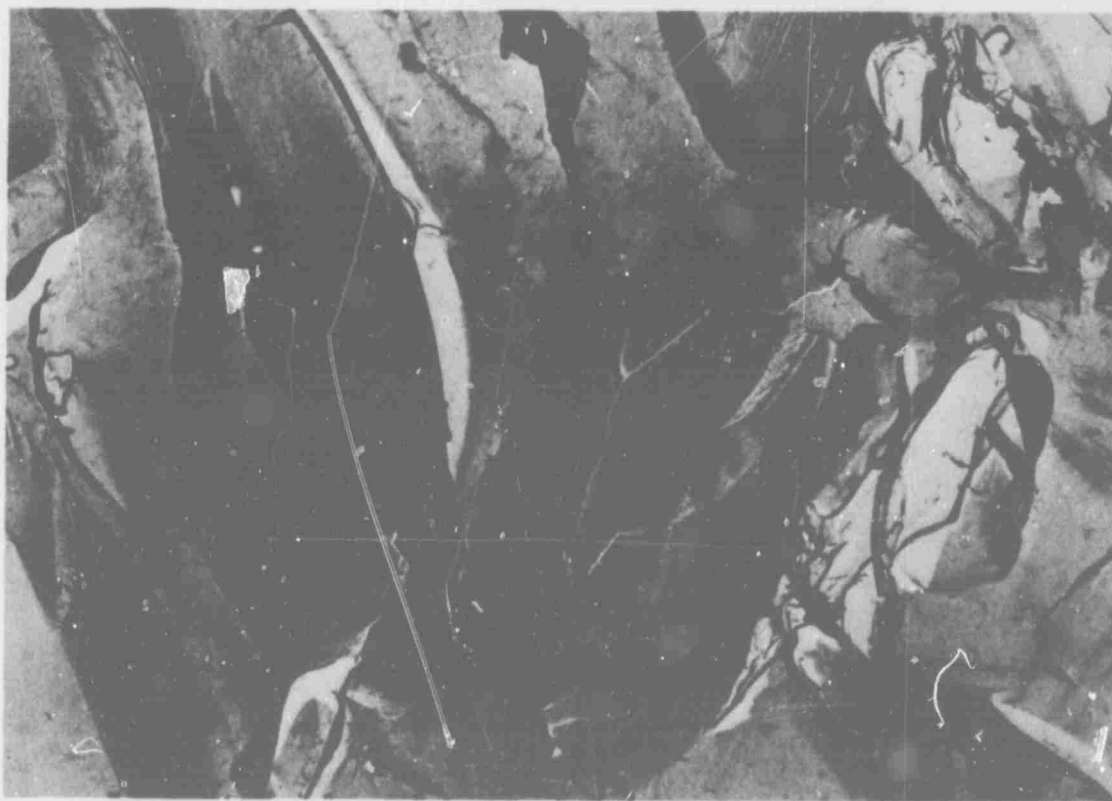
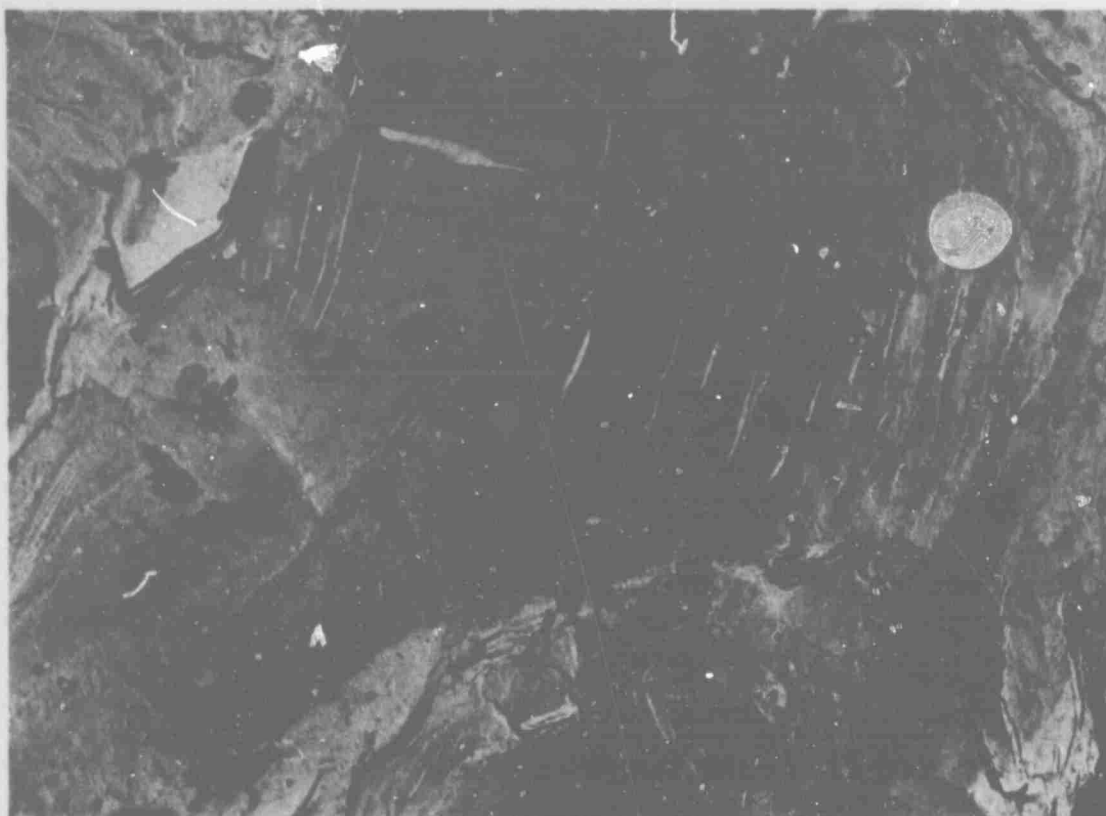


FIGURE 17(A). C 355 CYCLES TO FRACTURE — 15

EDGE OF
FRACTURE
SURFACE

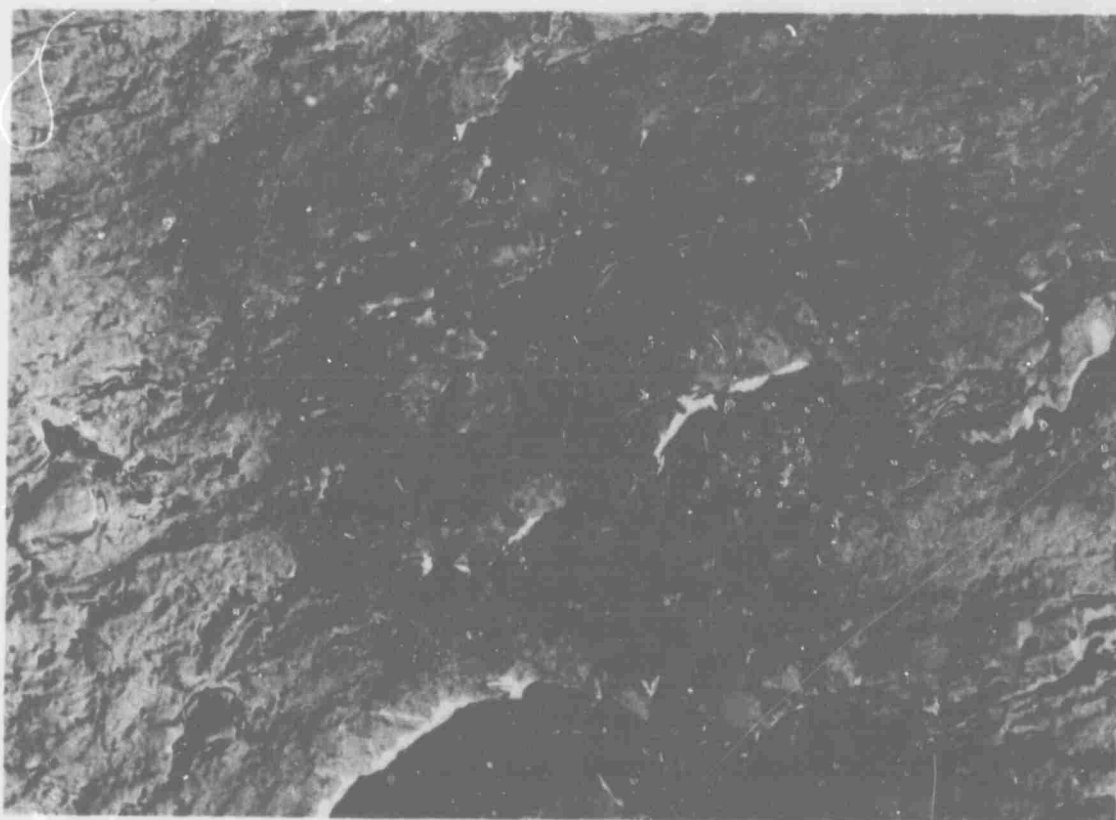


CENTER OF
FRACTURE
SURFACE



FIGURE 17(B). C 355 CYCLES TO FRACTURE - 147

EDGE OF
FRACTURE
SURFACE



CENTER OF
FRACTURE
SURFACE

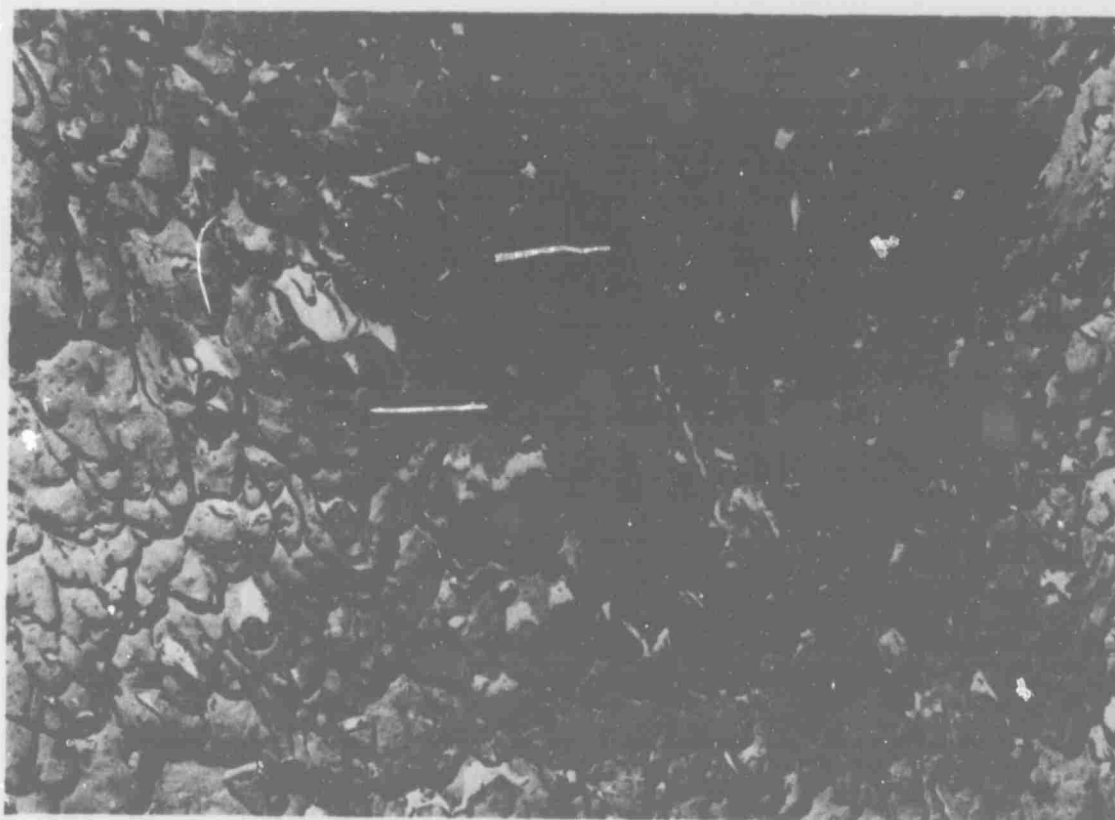
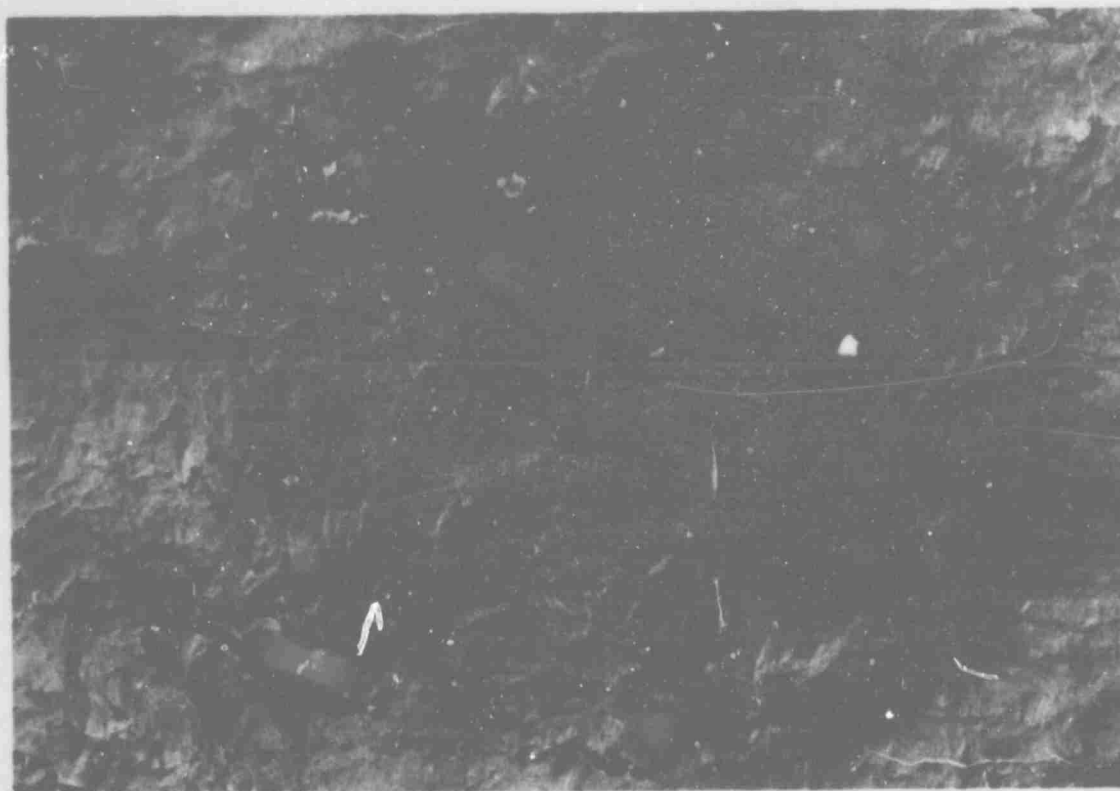


FIGURE 17(C). SAE 4340 CYCLES TO FRACTURE — 2552

EDGE OF
FRACTURE
SURFACE



CENTER OF
FRACTURE
SURFACE



FIGURE 17(D). SAE 4340. CYCLES TO FRACTURE-211

Table 1 Chemical Composition of SAE 4340 Steel Alloy, %

<u>C</u>	<u>Mn</u>	<u>Si</u>	<u>P</u>	<u>S</u>	<u>Cr</u>	<u>Mo</u>	<u>Fe</u>
0.28-0.33	0.40-0.60	0.20-0.35	0.04 Max.	0.04 Max.	0.80-1.1	0.15-0.25	Balance

Table 2 Chemical Composition of C355-T61 Aluminum Alloy, %

<u>Cu</u>	<u>Fe</u>	<u>Si</u>	<u>Mn</u>	<u>Mg</u>	<u>Zn</u>	<u>Cr</u>	<u>Ti</u>	<u>Al</u>
1.0-1.5	0.2	4.5-5.5	0.3 Max.	0.4-0.6	0.2 Max.	0.08	0.30	Balance

Table 3 Mechanical Properties of SAE 4340 Steel Alloy

<u>Group</u>	<u>0.2% Yield Strength, psi</u>	<u>Ultimate Tensile Strength, psi</u>	<u>Elongation Percent</u>	<u>Reduction in Area Percent</u>
A	103,000	126,000	20	61
B	114,000	134,000	16	53
C	132,000	147,000	14	45

Table 4 Mechanical Properties of C355-T61 Aluminum Alloy

<u>0.2% Yield Strength, psi</u>	<u>Ultimate Tensile Strength, psi</u>	<u>Elongation Percent</u>	<u>Reduction in Area Percent</u>
35,000	49,000	8	10

Table 5

Summary of SAE 4340 Rotor Test Results

Specimen Number	Surface Condition	Cyclic Speed Range, RPM	Cyclic Strain Range, μ "/"	Mean Strain μ "/"	Number of Cycles
S01A (1)	Polished	0-55800	-	297000	1/4
S02A	"	0-54000	5360	192000	5
S03A	"	0-52000	4630	116000	739
S04A	"	0-53000	4840	148000	371
S05A	"	0-53500	4940	168000	120
S06A	"	0-54000	5360	192000	6
S07A	"	0-53000	4840	148000	95
S08A	"	0-52000	4630	116000	827
S09A	"	0-51000	4420	87000	1286
S10A	Notched	0-51000	-	428000	1/4
S11A	"	0-49000	5346	274000	37
S12A	"	0-48000	5079	198000	144
S13A	"	0-47000	4810	140000	492
S14A	"	0-46000	4600	114000	714
S15A	"	0-50000	5615	350000	8
S16A	"	0-48000	5079	198000	96
S17A	"	0-49000	5346	274000	46
S18A	"	0-50000	5615	350000	3

(1) Indicates Group

Table 5 (continued)

Specimen Number	Surface Condition	Cyclic Speed Range, RPM	Cyclic Strain Range μ "/"	Mean Strain μ "/"	Number of Cycles
S19B	Polished	0-56200	-	264000	1/4
S20B	"	32600-54200	3360	148300	1897
S21B	"	31500-55100	3680	192100	39
S22B	"	0-55200	-	200000	1/2
S23B	"	42000-54100	2084	144900	184
S24B	"	44000-53000	1550	102200	10000 (2)
S25B	"	38500-54200	2600	148700	7225
S26B	"	20500-53200	4500	147700	40
S27B	"	20500-53200	4200	107300	1230
S28B	"	13800-53200	4620	107700	379
S29B	"	19800-54500	4620	163700	79
S30B	"	10000-55000	5280	187300	6
S31B	"	10000-55000	5280	187300	20
S32B	"	20500-54200	4500	147700	34
S33B	"	10000-54200	5080	147400	50
S34B	Notched	33000-50000	3110	193400	2552
S35B	"	31700-50800	3480	254200	211
S36B	"	30900-51400	3740	301100	48
S37B	"	30500-51900	3910	338000	12

(2) Retired

Table 5 (continued)

Specimen Number	Surface Condition	Cyclic Speed Range, RPM	Cyclic Strain Range μ "/"	Mean Strain μ "/"	Number of Cycles
S38B	"	0-51200	-	288000	1/4
S39B	"	31950-50350	3320	222300	1164
S40B	"	20000-50500	4720	283600	136
S41C	Polished	0-57800	-	204000	1/4
S42C	Polished	0-57600	-	193000	1/4
S43C	"	31500-56000	3620	118600	61
S44C	"	0-56000	5300	117600	10
S45C	"	0-54000	4840	58500	860
S46C	"	0-55000	5070	78300	181
S47C	"	30000-55000	3570	79000	1378
S48C	"	0-55000	5070	78300	35
S49C	"	0-56000	5300	117600	20
S50C	Notched	0-52600	-	293000	1/4
S51C	"	0-51000	5660	187800	46
S52C	"	0-50000	5530	156400	411
S53C	"	25000-51000	4300	188500	367
S54C	"	25000-51000	4300	188100	74
S55C	"	15000-51000	5170	187800	67
S56C	"	0-53300	-	304000	1/4

Table 6Summary of C355 Rotor Test Results

Specimen Number	Surface Condition	Cyclic Speed Range, RPM	Cyclic Strain Range μ "/"	Mean Strain μ "/"	Number of Cycles
L01	Polished	0-50500	3470	7460	90
L02	"	0-52500	3680	13560	2165
L03	"	0-56500	4120	37940	205
L04	"	0-54000	3830	19680	1106
L05	"	0-57100	4190	45100	94
L06	"	0-58600	-	69700	1/4
L07	"	0-56000	4050	32900	1067
L08	"	0-57500	4260	51470	26
L09	"	0-58000	4320	57840	15
L10	Notched	0-49000	4550	81565	1/4
L11	"	0-59000	4250	51050	229
L12	"	0-48000	4127	37630	367
L13	"	0-50000	4370	62130	147
L14	"	0-49300	4285	52850	1/4
L15	"	0-47000	4000	28980	349
L16	"	0-46000	3870	21450	903
L17	"	0-50000	4370	62130	27

Table 7

Exponents of Strain to Life Dependency

Elastic Strain - b Value

Material	Group	Surface Condition	Mean - Strain $\mu''/''$	b	b _{ave}
SAE 4340	B	polished	147000	9.25	
	B	polished	107000	8.50	
	C	polished	79000	9.70	9.15
SAE 4340	B	notched	215000	7.80	
	C	notched	188000	7.80	7.80

Plastic Strain - a Value

Material	Group	Surface Condition	Cyclic - Strain $\mu''/''$	a	a _{ave}
SAE 4340	A	polished	4840	3.00	
	B	polished	4900	2.96	
	C	polished	5070	3.80	3.25
	A	notched	5080	2.50	
	B	notched	3480	3.80	3.10
C355	-	polished	3970	3.75	
	-	notched	4160	2.20	

Table 8

Cumulative Damage Test ResultsSAE 4340

Specimen Number	Surface Condition	Cyclic Speed Range - RPM	Cyclic Strain Range - $\mu''/''$	n	N	n/N	$\Sigma n/N$
S57C	polished	0-56000	5301	1	15	0.06	
		0-54200	4983	351	700	0.50	0.56
S58C	"	0-56000	5301	3	15	0.20	
		0-54200	4983	551	700	0.79	0.99
S59C	"	0-56000	5301	6	15	0.40	
		0-54200	4983	159	700	0.23	0.63
S60C	"	0-56000	5301	1	15	0.06	
		0-54000	4930	324	720	0.46	0.52
S61C	"	0-55000	5072	6	181	0.03	
		0-54000	4840	700	860	0.81	
		0-55000	5072	79	181	0.43	1.27
S62C	"	0-56000	5301	6	15	0.40	
		0-55000	5142	51	175	0.29	0.69
S63C	"	0-55000	5072	51	175	0.29	
		0-56000	5301	19	15	1.26	1.55
S64C	"	0-56000	5301	6	15	0.40	
		20000-56000	4633	35	36	0.97	1.37
S65C	"	0-56000	5301	3	15	0.20	
		30000-56000	3785	64	150	0.43	0.63

Table 8 (continued)

Specimen Number	Surface Condition	Cyclic Speed Range - RPM	Cyclic Strain Range - $\mu''/''$	n	N	n/N	$\Sigma n/N$
S66C	"	0-56000	5301	8	15	0.53	
		30000-56000	3785	104	150	0.69	1.22
S67C	"	0-55000	5072	101	181	0.56	
		0-54000	4869	820	860	0.95	1.51
		Ave.				0.99	
S68C	Notched	25000-51000	4300	227	367	0.62	
		0-51000	5661	112	46	2.44	3.06
S69C	"	0-51000	5661	20	46	0.43	
		25000-51000	4300	227	367	0.62	1.05
S70C	"	0-50000	5529	261	411	0.63	
		0-51000	5661	7	46	0.15	0.78
S71C	"	15000-51000	5170	30	67	0.45	
		0-51000	5661	81	46	1.76	2.21
S72C	"	0-50000	5529	156	411	0.38	
		0-51000	5661	27	46	0.59	0.97
S73C	"	25000-51000	4300	100	367	0.27	
		0-51000	5661	33	46	0.72	0.99
S74C	"	0-51000	5661	20	46	0.43	
		0-50000	5460	261	430	0.61	1.04
		Ave.				1.44	

APPENDIX

Referring to figure 1a, when subscripts n and $n-1$ refer to the n th and $(n-1)$ st station on the rotor, the compatibility and equilibrium equation for each element is

$$\epsilon_{\theta, n} - r_{n-1} \epsilon_{\theta, n-1} / r_n - (r_n - r_{n-1}) (\epsilon_{r, n} + \epsilon_{r, n-1}) / 2 r_n = 0 \quad (1a)$$

$$\sigma_{\theta, n} - 2 r_n \sigma_{r, n} / r_n - r_{n-1} + 2 h_{n-1} r_{n-1} \sigma_{r, n-1} / h_n (r_n - r_{n-1}) + h_{n-1} \sigma_{\theta, n-1} / h_n - \rho \omega^2 (h_{n-1} r_{n-1}^2 / h_n + r_n^2) = 0 \quad (2a)$$

where changes due to deformation are neglected

Strains are related to stresses considering plane stress through the following relationships

$$\epsilon_{r, n} = (\sigma_{r, n} - \mu_n \sigma_{\theta, n}) / E_n + \bar{\epsilon}_{p, n} (\sigma_{r, n} - \sigma_{r, n} / 2) / \bar{\sigma}_n \quad (3a)$$

$$\epsilon_{\theta, n} = (\sigma_{\theta, n} - \mu_n \sigma_{r, n}) / E_n + \bar{\epsilon}_{p, n} (\sigma_{\theta, n} - \sigma_{r, n} / 2) / \bar{\sigma}_n \quad (4a)$$

where $\bar{\epsilon}_p$ and $\bar{\sigma}$ are defined by equations (20) and (21), respectively, in the test and denoted as equivalent strain and equivalent stress. The two additional relationships of the von Mises theory used to obtain equations (3a) and (4a) are

$$\epsilon_{\theta p} + \epsilon_{rp} + \epsilon_{zp} = 0 \quad (5a)$$

APPENDIX (Cont.)

or volume changes resulting from plastic flow are zero

and

$$(\epsilon_{rp} - \epsilon_{\theta p}) / (\sigma_r - \sigma_{\theta}) = (\epsilon_{rp} - \epsilon_{zp}) / \sigma_r = (\epsilon_{\theta p} - \epsilon_{zp}) / \sigma_{\theta} \quad (6a)$$

or principal plastic shear strains are assumed proportional to principal shear stresses. For this plane stress case, equations (20) and (21) yield

$$\bar{\sigma} = (\sigma_r^2 + \sigma_{\theta}^2 - \sigma_r \sigma_{\theta})^{1/2} \quad (7a)$$

$$\bar{\epsilon}_p = (\epsilon_{rp}^2 + \epsilon_{\theta p}^2 + \epsilon_{rp} \epsilon_{\theta p})^{1/2} / (3)^{1/2} \quad (8a)$$

Equivalent stress is related to equivalent strain by means of a true stress-true strain curve generated from a uniaxial tensile test of the subject material.

Equations (1a) through (8a) are solved using an iterative technique. The solution of any rotor station, n , in terms of values at the preceding station, $n-1$, are obtained. Hence, the solution for the entire rotor can be obtained in terms of an assumed quantity at the center. A comparison of the radial stress at the last station with the rim loading, which is readily calculable quantity, indicates whether or not an adjustment in the assumed quantity at the center is warranted.

APPENDIX (Cont.)

Residual stresses and strains are determined by allowing the rotor to recover elastically from the stress and strain state at maximum speed.

Compressive residual stress values must be examined to assure that they do not exceed the compressive yield point of the material. Otherwise, elastic recovery is not justified.

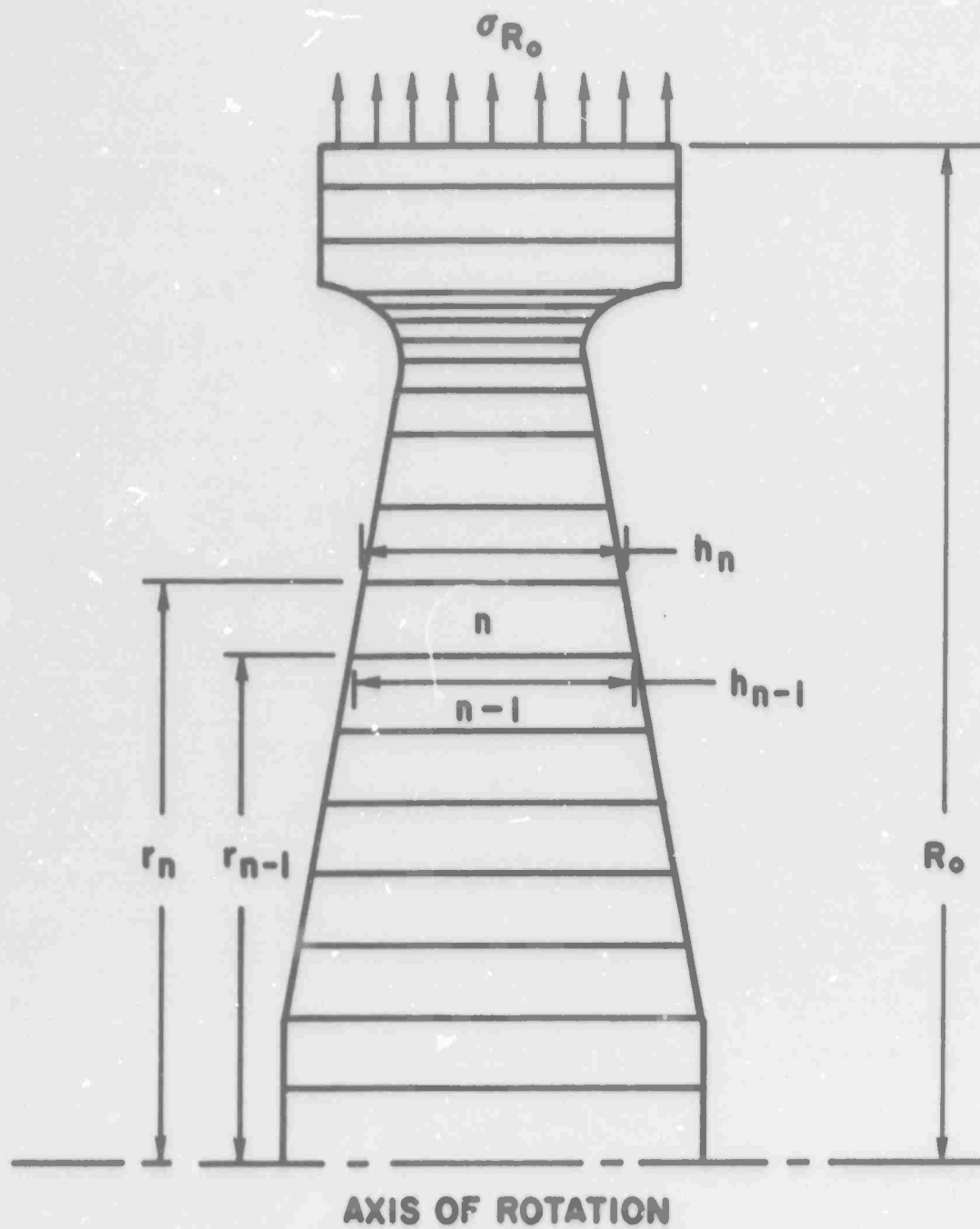


FIGURE 1A. ROTOR ANALYSIS COORDINATE SYSTEM

REFERENCES

1. S. S. Manson, "Behavior of Materials under Conditions of Thermal Stress, Heat Transfer," Symp. Univ. Mich. Eng. Res. Inst., 1953, pp. 9-75.
2. S. S. Manson, "Behavior of Materials under Conditions of Thermal Stress," NASA Tech. Note 2933, 1954.
3. L. F. Coffin, Jr. "A Study of Cyclic-Thermal Stresses in a Ductile Metal," Trans. ASME, vol. 76, 1954, pp. 931-950.
4. L. F. Coffin, Jr. and J. F. Tavernelli, "Cyclic Straining and Fatigue of Metals," Trans. Met. Soc. AIME, vol. 215, no. 5, October, 1959, pp 794-807.
5. J. F. Tavernelli and L. F. Coffin, "Experimental Support for Generalized Equation Predicting Low Cycle Fatigue", J. Basic Engineering, vol. 84, no. 4, December, 1962, pp 533-541.
6. M. R. Gross, "Low Cycle Fatigue of Materials for Submarine Construction", Report 91-197D, U.S. Naval Engineering Experimental Station, Annapolis, Maryland, ASTIC No. 013146, February 14, 1963.
7. K. D. Ives, L. F. Koolstra, and J. T. Tucker, "Equibiaxial Low Cycle Fatigue Properties of Typical Pressure-Vessel Steels", J. Basic Engineering, vol. 88, no. 4, December, 1966 pp. 745-753.

REFERENCES (Cont'd)

8. T.H. Plan and R. D'Amato, "Low Cycle Fatigue of Notched and Unnotched Specimens of 2024 Aluminum Alloy Under Axial Loading," WADC Technical Note 58-27, Wright Air Development Center, Wright Patterson Air Force Base, Ohio, 1958.
9. R. D'Amato and R. DeBoer, "A Study of the Relationship Between Notched and Unnotched Specimens of 2024 Aluminum Alloy in the Low-Cycle Fatigue Regime," WADC Technical Note 59-2, Wright Air Development Center, Wright Patterson Air Force Base, Ohio, May, 1959.
10. G. Sachs, W.W. Gerberich, V. Weiss and J. V. Latorre, "Low Cycle Fatigue of Pressure Vessel Materials," Proceedings ASTM, vol. 60, 1961, pp. 512-529.
11. H. Ohji, W.R. Miller, and J. Marin, "Cumulative Damage and Effect of Mean Strain in Low-Cycle Fatigue of a 2024-T351, Aluminum Alloy," J. Basic Engineering, Trans. ASME, vol. 88, no. 4, pp. 801-810.
12. M.A. Miner, "Cumulative Damage in Fatigue," J. Applied Mechanics, vol. 12, Trans. ASME 1945, pp. 159-164.
13. J. H. Gross and R. D. Stout, "Plastic Fatigue Properties of High Strength Pressure Vessel Steels", Research Supplement, vol. 34, 1955, pp. 161-166.

REFERENCES (Cont.)

14. E.E. Baldwin, G. Sokol, and L.F. Coffin, Jr. "Cycle Strain Fatigue Studies on AISI Type 347 Stainless Steel," Proceedings ASTM, vol. 57, 1958, pp. 587-586.
15. R.D'Amato, "A Study of the Strain Hardening and Cumulative Damage Behavior of 2032-T4 Aluminum Alloy in the Low Cycle Fatigue Range," WADD Tech. Note 60-175, Wright Air Development Division, Wright Patterson Air Force Base, Ohio, April, 1960.
16. D. E. Gucer, "Cumulative Fatigue at High Plastic Strains", Trans. ASM, vol. 54, 1961, pp. 176-184.
17. S. S. Manson, Thermal Stress and Low Cycle Fatigue, McGraw-Hill Book Co., New York, New York, 1966.
18. R. W. Smith, M. H. Hirshberg, and S. S. Manson, "Fatigue Behavior of Materials under Strain Cycling in Low and Intermediate Life Range," NASA Tech. Note D-1574, April, 1963.
19. S. S. Manson, "Thermal Stresses in Design, Part 21: Effect of Mean Stress and Strain on Cyclic Life; Part 22: Cumulative Fatigue Damage," Machine Design, vol. 32, August, 1960.
20. J. Dorn and E. G. Thomsen, "The Ductility of Metals Under Conditions of Stress and Strain," Trans. ASM, vol. 39, 1947, pp. 741-772.
21. S. S. Manson, "Analysis of Rotating Disks of Arbitrary Contour and Radial Temperature Distribution in the Region of Plastic Deformation," Proc. 1st Nat. Congr. App. Mech., ASME, 1951.

REFERENCES (Cont'd)

22. N. E. Waldren and D. E. Ward, "Room Temperature Instability and Fracture in Rotating Disks and Correlation with Biaxial Tensile Test Data," Aeronautical Research Council Current Paper No. 660, 1963.
23. N. E. Waldren, M. J. Percy and P. B. Mellor, "Burst Strength of Rotating Disks," Proc. Instn. Mech. Engrs., vol. 180, Pt 1, No. 5, 1965-1966.

(Unclassified)
Security Classification

DOCUMENT CONTROL DATA - R&D

(Security classification of title, body of abstract and indexing annotation must be entered when the overall report is classified)

1. ORIGINATING ACTIVITY (Corporate author)		2a. REPORT SECURITY CLASSIFICATION	
United Aircraft Corporation		Unclassified	
		2b. GROUP	
		NA	
3. REPORT TITLE			
LOW CYCLE FATIGUE BEHAVIOR UNDER BIAXIAL STRAIN DISTRIBUTION			
4. DESCRIPTIVE NOTES (Type of report and inclusive dates)			
Final Report			
5. AUTHOR(S) (Last name, first name, initial)			
Mattavi, Joseph L.			
6. REPORT DATE		7a. TOTAL NO. OF PAGES	7b. NO. OF REFS
September 1967		56	23
8a. CONTRACT OR GRANT NO.		9a. ORIGINATOR'S REPORT NUMBER(S)	
DA-31-124-ARO-D-274			
b. PROJECT NO.			
20014501B33G			
c.		9b. OTHER REPORT NO(S) (Any other numbers that may be assigned this report)	
d.		4872.3-E	
10. AVAILABILITY/LIMITATION NOTICES This document is subject to special export controls and each transmittal to foreign governments or foreign nationals may be made only with prior approval of the U.S. Army Research Office-Durham, Durham, North Carolina.			
11. SUPPLEMENTARY NOTES		12. SPONSORING MILITARY ACTIVITY	
None		U.S. Army Research Office-Durham Box CM, Duke Station Durham, North Carolina 27706	
13. ABSTRACT			
<p>> 76 This paper presents a linear cumulative damage theory, macroscopically considering elastic and plastic straining, and accounting for biaxiality through the von Mises theory for combined strains. Experimentation on SAE 4340 steel alloy supported this damage hypothesis and confirmed the associated exponential relationship between elastic strains with cyclic life and plastic strains with cyclic life. A limited evaluation of an aluminum casting material, C-355-T61, also supported this exponential dependency. Notching did not significantly alter this low cycle fatigue behavior.</p>			
14. KEY WORDS		linear cumulative damage theory low cycle fatigue elastic straining plastic straining steel alloy cyclic life exponential dependency notching	

DD FORM 1 JAN 64 1473

Unclassified
Security Classification